

Ocean Observations in Support of Studies and Forecasts of Tropical and Extratropical Cyclones

Ricardo Domingues^{1,2*}, Akira Kuwano-Yoshida³, Patricia Chardon-Maldonado^{4,5}, Robert E. Todd⁶, George R. Halliwell², Hyun-Sook Kim^{7,8}, I-I Lin⁹, Katsufumi Sato¹⁰, Tomoko Narazaki¹⁰, Lynn K. Shay¹¹, Travis Miles¹², Scott Glenn¹², Jun A. Zhang^{1,2}, Steven R. Jayne⁶, Luca R. Centurioni¹³, Matthieu Le Hénaff^{1,2}, Gregory Foltz², Francis Bringas², MM Ali¹⁴, Steven DiMarco¹⁵, Shigeki Hosoda¹⁶, Takuya Fukuoka¹⁰, Benjamin LaCour¹⁷, Avichal Mehra⁷, Elizabeth R. Sanabia¹⁸, John R. Gyakum¹⁹, Jili Dong⁷, John Knaff¹⁷, Gustavo J. Goni²

¹Cooperative Institute for Marine and Atmospheric Studies (CIMAS), United States, ²Atlantic Oceanographic and Meteorological Laboratory (NOAA), United States, ³Kyoto University, Japan, ⁴University of Puerto Rico at Mayagüez, Puerto Rico, ⁵Caribbean Regional Association for Integrated Coastal Ocean Observing, University of Puerto Rico at Mayagüez, Puerto Rico, ⁶Woods Hole Oceanographic Institution, United States, ⁷National Weather Service, United States, ⁸I.M. Systems Group, Inc., United States, ⁹National Taiwan University, Taiwan, ¹⁰The University of Tokyo, Japan, ¹¹Rosenstiel School of Marine and Atmospheric Science, University of Miami, United States, ¹²Rutgers University, The State University of New Jersey, United States, ¹³Scripps Institution of Oceanography, University of California, San Diego, United States, ¹⁴International CLIVAR Global Project Office, China, ¹⁵Texas A&M University Central Texas, United States, ¹⁶Japan Agency for Marine-Earth Science and Technology, Japan, ¹⁷National Oceanic and Atmospheric Administration (NOAA), United States, ¹⁸United States Naval Academy, United States, ¹⁹McGill University, Canada

Submitted to Journal:
Frontiers in Marine Science

Specialty Section:
Ocean Observation

Article type:
Review Article

Manuscript ID:
437868

Received on:
20 Nov 2018

Frontiers website link:
www.frontiersin.org

Conflict of interest statement

The authors declare that the research was conducted in the absence of any commercial or financial relationships that could be construed as a potential conflict of interest

Author contribution statement

RD, AKY, PCM, and GG elaborated the initial outline, and wrote the first draft of the manuscript.

All 29 authors of this community white paper have provided input in the form of language, figures, and recommendations for the future of the ocean observing system in support of studies and forecasts of Tropical and Extratropical Cyclones.

Keywords

Weather extremes, Global Ocean Observing System (GOOS), Coupled Ocean-Atmosphere Weather Forecasts, ocean heat content (OHC), Barrier layer, Western boundary currents, Mesoscale Ocean Features

Abstract

Word count: 196

Over the past decade, the climate-oriented ocean observing system has provided datasets crucial for advancing our understanding of extreme weather events that originate and intensify over the ocean, such as tropical cyclones (TCs) and extratropical bomb cyclones (EBCs). Despite these advances, a component of the ocean observing system dedicated specifically in support of studies and forecasts of TCs and EBCs is yet to be implemented. New technologies, pilot networks, targeted deployments of instruments, and state-of-the-art coupled numerical forecast models have enabled advances in research and forecast capabilities and illustrate a potential framework for the future. In this community white paper, we discuss the applications and key results made possible by the different ocean observing efforts in support of studies and forecasts of TCs and EBCs. The paper describes the recent advances in observing technologies and strategies in light of previous recommendations from the scientific community during OceanObs'09, and provides a vision and specific recommendations for the next decade. The need for a sustained component within the ocean observing system dedicated specifically to help improve TCs and EBCs forecasts was identified by the community as a key recommendation to be addressed during the upcoming decade.

Data availability statement

Generated Statement: No datasets were generated or analyzed for this study.

Ocean Observations in Support of Studies and Forecasts of Tropical and Extratropical Cyclones

Ricardo Domingues^{1,2,*}, Akira Kuwano-Yoshida³, Patricia Chardon-Maldonado^{4,5}, Robert E. Todd⁶, George Halliwell², Hyun-Sook Kim^{2,7}, I-I Lin⁸, Katsufumi Sato⁹, Tomoko Narazaki⁹, Lynn K. Shay¹⁰, Travis Miles¹¹, Scott Glenn¹¹, Jun A. Zhang^{1,2}, Steven R Jayne⁶, Luca Centurioni¹¹, Matthieu Le Hénaff^{1,2}, Gregory R. Foltz², Francis Bringas², MM Ali¹³, Steven F. DiMarco¹⁴, Shigeki Hosoda¹⁵, Takuya Fukuoka⁹, Benjamin LaCour², Avichal Mehra², Elizabeth R. Sanabia¹⁶, John R. Gyakum¹⁷, Jili Dong², John A. Knaff², Gustavo Goni²

¹ Cooperative Institute for Marine and Atmospheric Studies, University of Miami, USA

² National Oceanic and Atmospheric Administration, USA

³ Kyoto University, Japan

⁴ Caribbean Coastal Ocean Observing System, Puerto Rico

⁵ University of Puerto Rico, Puerto Rico

⁶ Woods Hole Oceanographic Institution, USA

⁷ I. M. Systems Group, Inc., Maryland, USA

⁸ National Taiwan University, Taiwan

⁹ University of Tokyo, Tokyo, Japan

¹⁰ Rosenstiel School of Marine and Atmospheric Science, University of Miami, USA

¹¹ Rutgers University, USA

¹² Scripps Institution of Oceanography, USA

¹³ International CLIVAR Global Project Office

¹⁴ Texas A&M University, USA

¹⁵ Japan Agency for Marine-Earth Science and Technology, Japan

¹⁶ United States Naval Academy, USA

¹⁷ McGill University, Canada

* corresponding author: Ricardo.Domingues@noaa.gov

Abstract: Over the past decade, the climate-oriented ocean observing system has provided datasets crucial for advancing our understanding of extreme weather events that originate and intensify over the ocean, such as tropical cyclones (TCs) and extratropical bomb cyclones (EBCs). Despite these advances, a component of the ocean observing system dedicated specifically in support of studies and forecasts of TCs and EBCs is yet to be implemented. New technologies, pilot networks, targeted deployments of instruments, and state-of-the art coupled numerical forecast models have enabled advances in research and forecast capabilities and illustrate a potential framework for the future. In this community white paper, we discuss the applications and key results made possible by the different ocean observing efforts in support of studies and forecasts of TCs and EBCs. The paper describes the recent advances in observing technologies and strategies in light of previous recommendations from the scientific community during OceanObs' 09, and provides a vision and specific recommendations for the next decade. The need for a sustained component within the ocean observing system dedicated specifically to help improve TCs and EBCs forecasts was identified by the community as a key recommendation to be addressed during the upcoming decade.

Keywords: Weather Extremes, Global Ocean Observing system, Coupled Ocean-Atmosphere Weather Forecasts, Ocean Heat Content, Barrier Layers, Western Boundary Currents, Mesoscale Ocean Features.

49 **1. Introduction**

50 Extreme weather events are natural hazards that affect marine and land areas around the
51 world and are associated with different temporal and spatial scales (Elsner et al. 2008; Menkes et
52 al. 2016; Zhou et al. 2018). Tropical cyclones (TCs), and their extratropical counterpart, often
53 referred as extratropical “bomb” cyclones (EBCs), are deep low pressure systems that produce
54 and sustain high intensity winds generated over the ocean (TCs) or predominantly over the ocean
55 (EBCs). TCs and EBCs are among the deadliest and costliest types of extreme weather that often
56 cause widespread damage due to their strong winds, storm surge, and heavy precipitation, posing
57 risks to human lives and infrastructure. Understanding their dynamical mechanisms and having
58 the ability to accurately forecast them is, therefore, a critical societal need, and remains a
59 challenge. Some topics that will be addressed here relate to the impact of ocean observations on
60 the forecasting of TC and EBC intensity. One of the main purposes of this article is to discuss
61 and recommend potential observation strategies for future TC and EBCs forecasting and
62 research.

63 The understanding of upper-ocean processes leading to extreme weather events, such as
64 TCs and EBCs, has largely benefited from the climate-oriented sustained ocean observing
65 system and observational process studies. Clearly, ocean observations are vital in EBCs and TCs
66 research, especially with the more and more occurrences of record-breaking “Cat-6” types of
67 TCs (e.g. Lin et al. 2014; Rogers et al. 2017; Huang et al. 2017). In addition, recent advances in
68 research and ocean observing efforts have largely addressed specific recommendations identified
69 by the scientific community during OceanObs’ 09 (e.g., Goni et al., 2010) about key areas to be
70 addressed in the upcoming decade in support of TCs studies and forecasts. Since then, new
71 technologies, pilot networks, and targeted deployments have further expanded the reach of the
72 global observing system and have been used in weather analyses, outlooks, and improved ocean-
73 atmosphere numerical forecasts models. For instance, (i) extensive synergies between the
74 scientific and operational communities continue facilitating transitions of research results into
75 operations (e.g., Shay et al., 2014); (ii) networks specifically designed in support of TC studies
76 and forecasts have been implemented (e.g., Domingues et al., 2015; Miles et al., 2015) (iii)
77 targeted airborne profiling observations ahead of forecasted TCs have since then been
78 extensively implemented (e.g., D’Asaro et al., 2014; Jaimes et al., 2016; Meyers et al., 2015;
79 Zhang et al., 2018); (iv) substantial progress has been accomplished on understanding the role of
80 upper ocean salinity (e.g., Balaguru et al. 2012a, b; Domingues et al. 2015) and temperature
81 stratification (Price 2009; Lin et al. 2013b, a; Balaguru et al. 2015, 2018; Glenn et al. 2016) for
82 sustaining TC intensity and changes; (v) real-time assimilation of ocean observations into
83 coupled weather forecast systems continues providing critical information for improved ocean
84 representation (e.g., Dong et al., 2017), and (vi) new state-of- the-art coupled numerical forecast
85 weather models have evolved and are now being used in experimental and operational modes
86 (e.g., Kim et al., 2014).

87 In this community white paper, we describe some of the most important advances in the
88 observational efforts in support of studies and forecasts of TCs and EBCs since OceanObs' 09,
89 and present and discuss some potential enhancements to ocean observing strategies for the
90 upcoming future, as well as provide specific recommendations.

91

92 **1.1 Tropical Cyclones**

93 A TC is a fast-rotating storm system that is characterized by a low pressure center that
94 forms in the tropics. TCs are observed in seven ocean basins worldwide (Figure 1), namely the:
95 tropical Atlantic, northeast Pacific, northwest Pacific, southwest Indian, north Indian, southeast
96 Indian, and south Pacific. In the North Atlantic Ocean basin, for example, 11 named TCs, 6
97 hurricanes, and 2-3 major hurricanes are generally observed to develop from June to November
98 in a typical year (Landsea, 1993). In general, sea surface temperatures (SSTs) above 26°C are
99 needed for Atlantic hurricane generation (e.g., Leipper and Volgenau 1972). With respect to the
100 intensity changes of TCs, the vertical thermal structure (e.g., Leipper and Volgenau, 1972; Shay
101 et al., 2000; Mainelli et al., 2008; Goni et al., 2009; Shay and Brewster, 2010) and the
102 stratification of the upper ocean (e.g., Lin et al., 2008; Price, 2009; Balaguru et al., 2012a, 2012b,
103 2015; Domingues et al., 2015; Emanuel, 2015; Huang et al., 2015; Seroka et al., 2016; Rudzin et
104 al., 2017, 2018) have been shown to be important factors that may contribute with intensification
105 and weakening of TCs, provided that the atmospheric conditions are also favorable. Intense
106 upper ocean mixing events caused by the strong hurricane winds can quickly erode the thermal
107 signature of subsurface warm or cold features (Pickard and Emery, 1990), leading to SST
108 misrepresenting the ocean thermal energy. Several studies (e.g., Mao et al., 2000; Shay et al.,
109 2000; Ali et al., 2007, 2013; Mainelli et al., 2008; Lin et al., 2013b) demonstrated the importance
110 of ocean thermal energy, represented by warm ocean features. In addition, the stratification of
111 the upper ocean, including the waters below the mixed layer, and the storm maximum wind and
112 translation speed have been also shown to be linked to hurricane intensification (Balaguru et al.,
113 2018).

114 The intensification of TCs includes the interaction of very complex mechanisms at multi-
115 scales, such as internal TC dynamics, upper ocean interaction, and atmosphere circulation. Rapid
116 intensification is often associated with TCs moving over warm ocean features (i.e. SSTs larger
117 than 26°C, Figure 2), which maintain warmer sea surface temperatures (due to suppression of
118 TC-induced sea surface cooling) near the convective center of the TC (Shay et al., 2000; Goni
119 and Trinanes, 2003; Lin et al., 2005, 2009); thermal energy across the sea surface is central to the
120 enthalpy fluxes that transport heat and moisture from the ocean to the atmosphere, fueling the
121 TC. For this reason, ocean heat content (OHC) estimates from a variety of datasets and
122 methodologies are routinely used to provide operational guidance for intensity change and rapid
123 intensification (e.g., Goni and Trinanes, 2003; DeMaria et al., 2005; Kaplan et al., 2010; Shay
124 and Brewster, 2010; Meyers et al., 2014; Rogers et al., 2017; Knaff et al., 2018; Yamaguchi et

125 al., 2018). Despite these advances in understanding the role that the upper ocean plays in TC
126 intensification, short-term intensity forecast errors have not been significantly reduced over the
127 past two decades in any basin (DeMaria et al., 2007, 2014), particularly in the Atlantic basin
128 (Figure 3). One of the factors contributing to the lag in improvement of TC intensity forecasts
129 relative to TC track forecasts may be the lack of a dedicated ocean observing system with
130 sustained and targeted ocean observations to correctly represent the ocean component in ocean-
131 atmosphere coupled intensity forecast models.

132

133 **1.2. Extratropical Bomb Cyclones**

134 An EBC is an extratropical cyclone that undergoes rapid deepening of its low pressure by
135 24 mbar or more in a period of 24 hours or less. This process is predominantly maritime, taking
136 place in winter, with seldom occurrences over continental land masses. Atmospheric baroclinic
137 instabilities, upper levels vorticity coupling and diabatic processes have been acknowledged as
138 the main mechanisms causing EBCs genesis (Shapiro et al. 1999; Yoshida and Asuma 2004;
139 Kuwano-Yoshida and Asuma 2008). Even though their genesis involves processes completely
140 different from that of TCs, EBCs still produce winds as strong as hurricanes and are often
141 associated with large rain events. The strength, intensification and trajectory of the EBCs are
142 known for being influenced by upper ocean conditions (Kuwano-Yoshida and Minobe, 2017).
143 For example, genesis of EBCs is often associated with upper ocean conditions at frontal systems,
144 such as at the Kuroshio or the Gulf Stream, which enables large heat fluxes from the ocean into
145 the storm (Sanders and Gyakum, 1980; Ulbrich et al. 2009; Hirata et al. 2015, 2016, 2018;
146 Kuwano-Yoshida and Minobe 2017). Future projections suggest that strong EBCs will tend to
147 increase, while the total number of extratropical cyclones is expected to decrease (Colle et al.
148 2015; Chang 2017). Some of these climate models projections, however, cannot fully resolve
149 sharp gradients linked with the Kuroshio and the Gulf Stream currents (Haarsma et al., 2016),
150 and therefore further studies are still required to confirm these trends.

151 The intensity of EBCs developing over warmer ocean are underestimated when compared
152 to those over cooler ocean (Kuwano-Yoshida and Enomoto, 2013), because latent heat release
153 associated with cloud condensation process is more important for rapid development than upper
154 vorticity forcing (Catto et al., 2010). Recent analysis using satellite based high-resolution SST
155 data suggest that EBCs are affected by SST fluctuations associated with fronts and mesoscale
156 eddies around western boundary currents (Booth et al., 2012; Kuwano-Yoshida and Minobe,
157 2017; Hirata et al., 2015; 2016; 2018). Considering that the western boundary currents such as
158 the Gulf Stream and the Kuroshio are warming more rapidly than global mean (Wu et al., 2012),
159 ocean effect on EBCs forecasts will increase in the future. With respect to ocean response to
160 EBCs winds, recent ocean simulations suggest that EBCs can induce surface horizontal
161 divergence and upwelling reaching depths of 6,000 m, which can impact the deep ocean

162 circulation and ecosystems through mixing and bio-geochemical transport (Kuwano-Yoshida et
163 al., 2017).

164

165 **2. Ocean Observations and Parameters in Support of Extreme Weather Studies and** 166 **Forecasts**

167 The Global Ocean Observing System (GOOS) provides valuable and unique datasets
168 derived from a diverse suite of observing platforms that enables us to partly address the
169 challenges of understanding the complex physical mechanisms associated with extreme weather,
170 their internal dynamics, and also to help improve the overall skill of extreme weather forecast
171 models. Accurate TC forecasts based on coupled models, for example, require a correct
172 representation of the upper-ocean heat content, vertical density structure, and the mesoscale
173 field. Similarly, the correct representation of upper ocean processes under ECBs require
174 returning observations with high spatial and temporal resolution.

175 Ocean observations of TCs and EBCs have enabled improved understanding about their
176 development and intensification, which occur over distinct geographic domains and on different
177 seasons. The GOOS includes several ocean observing efforts led by the international community
178 that are serving to support studies and forecasts of both TCs and EBCs. While the observational
179 requirements and needs for TCs and EBCs are different, some of these platforms are used in
180 support of studies on both events, and some are particularly used for TCs or EBCs.

181 We discuss here the importance of the integrated ocean observing system and of targeted
182 observations, focusing on its application to TCs and EBCs. We also provide an overview of these
183 components based on several successful examples of a suite of technologies and improved
184 capabilities that are helping accomplish the above objectives. Some of these platforms are being
185 used for targeted TC sampling and process studies, while others are components of the sustained
186 ocean observing system (Legler et al., 2015). Preferably, the data transmission from the
187 observing platforms requires to be carried out in near real-time, to be available to forecasters in a
188 timely manner (e.g. the Global Telecommunication System, GTS), and to use in operational
189 forecasts.

190

191 **2.1. Ocean Observations**

192 Satellites: Satellite-derived fields of SST¹ and of sea surface height (SSH)² are used to estimate
193 the upper ocean heat content (OHC, Leiper and Volgenau, 1972), which is sometimes also

¹NOAA High-resolution Blended Analysis of Daily SST available at :
<https://www.esrl.noaa.gov/psd/data/gridded/data.noaa.oisst.v2.highres.html>

194 referred to as Tropical Cyclone Heat Potential³ (TCHP; Goni and Trinanes, 2003). The
195 TCHP/OHC is defined as the excess heat content in the water column between the sea surface
196 and the depth of the 26°C isotherm. These TCHP/OHC fields can provide key qualitative and
197 quantitative spatial information of areas where TCs may intensify, mainly by identifying the
198 location and thermal characteristics of warm eddies and current frontal regions (Meyers et al.,
199 2014). For example, high values of TCHP (larger than approximately 50 kJ/cm²) have been
200 shown to be linked to intensification of Atlantic TCs (e.g., Mainelli et al., 2008). Fields of SST
201 and TCHP/OHC are now used by the National Oceanic and Atmospheric Administration
202 (NOAA) National Hurricane Center (NHC) and the Joint Typhoon Warning Center for their
203 subjective TC intensity forecasts and quantitatively in the Statistical Hurricane Intensity
204 Prediction Scheme (SHIPS) (DeMaria and Kaplan, 1994; DeMaria et al., 2005) and rapid
205 intensification aids (Kaplan et al., 2010; Knaff et al., 2018). Notable examples of use of satellite
206 fields to assess links between the ocean and hurricane intensification include Hurricane Opal
207 (Shay et al., 2000), super-typhoon Maemi (Lin et al., 2005), Hurricane Katrina (Figure 2; Goni et
208 al., 2009), and “killer cyclone” Nargis (Lin et al., 2009).

209 Underwater gliders: Autonomous underwater gliders (Rudnick, 2016) provide measurements of
210 temperature and salinity in the upper several hundred meters and are becoming key components
211 of the ocean observing system (Liblik et al., 2016; Testor et al., this issue). In addition to the
212 standard measurements of temperature, salinity, and depth-average currents, gliders can be
213 equipped to measure current profiles (e.g., Todd et al., 2017), bio-optical properties, dissolved
214 oxygen, and turbulent microstructure. Because of their adaptability and versatility, gliders can,
215 and are helping fill important observational gaps in the ocean observing system (Liblik et al.,
216 2016), particularly with respect to TC intensity forecasts. Glider observations are, for example,
217 frequently assimilated into ocean-atmosphere coupled models and used for intensity hurricane
218 forecasts. Sustained glider deployments are currently monitoring upper ocean conditions in areas
219 frequently impacted by TCs (e.g., Domingues et al., 2015; Miles et al., 2015; Todd et al. 2018).
220 In addition, gliders have particular utility measuring ocean processes on continental shelves
221 before and during landfalling of TCs, where alternative datasets are scarce (e.g., Glenn et al.,
222 2016; Miles et al., 2017). Since gliders move slowly (about 25 km/day) compared to most
223 atmospheric cyclones (100 km/day), actively piloting them into the paths of storms is generally
224 not feasible due to the short lead times of forecasts. Thus, sustained deployment of gliders at
225 locations prone to tropical or extratropical cyclones (e.g., Domingues et al., 2015, Glenn et al.,
226 2016; Perry et al., 2017) or along oceanic boundaries as part of boundary current observing
227 systems (Todd et al., 2018; Testor et al., this issue; Todd et al., this issue) is preferable.

²Satellite altimetry products made available by the Copernicus Marine Environment Monitoring Service:
<http://marine.copernicus.eu/>

³TCHP fields made available by the NOAA Atlantic Oceanographic and Meteorological Laboratory at:
<http://www.aoml.noaa.gov/phod/cyclone/data/>

228 Compared to rapid response deployments (e.g., Miles et al., 2015; Goni et al., 2017), sustained
229 glider surveillance has the distinct advantage of providing critical high resolution observations in
230 the open ocean and continental shelf break prior to storm arrival, which have been shown to
231 improve the representation of the ocean in operational coupled forecasts models of hurricane
232 intensity (e.g., Dong et al., 2017). Most underwater glider data are transmitted in real-time into
233 the GTS and U.S. Integrated Ocean Observing System (IOOS) underwater glider data assembly
234 center⁴.

235 *Surface Drifters:* Different types of drifters provide mostly sustained observations of ocean
236 current velocities, SST, and sea level pressure (SLP) that are also used in support of weather
237 forecasts, including TCs and EBCs. Sustained global observations from drifters are used for
238 constraining satellite SST errors and biases (e.g., Zhang et al., 2009) and have enabled a positive
239 impact on global weather forecast throughout the troposphere thanks to assimilation of in-situ
240 SLP observations (Centurioni et al. 2017; Horányi et al. 2017; Ingleby and Isaksen, 2018). The
241 Forecast Sensitivity to Observations Impact study results described by Horányi et al. (2017) have
242 also shown that, in case of intense cyclogenesis, SLP observations from drifters made possible
243 for large reduction in forecast errors, sometimes the largest among all the other assimilated
244 observations. Furthermore, targeted deployments of drifters are sometimes carried out in front of
245 TCs to measure surface currents, SSTs, sea level pressure, and surface winds. During the
246 Atlantic hurricane season, for example, Surface Velocity Program (SVP), Surface Velocity
247 Program Barometer (SVPB), and Autonomous Drifting Ocean Station drifters (Centurioni, 2010;
248 see also Centurioni et al., 2018, for a complete description of the drifter technology) are often
249 air-deployed in front of TCs that may impact the US mainland. New drifters capable of
250 measuring the directional wave spectra of surface gravity waves, termed the Directional Wave
251 Spectra Drifters (Centurioni et. al, 2016; Centurioni et al., this issue) have also been deployed
252 ahead of TCs. Successful deployments of various drifters have been carried out in the Atlantic
253 Ocean during the following TCs: Fabian (2003), Frances (2004), Rita (2005), Dean (2007),
254 Gustav (2008), Ike (2008), Isaac (2012) and Michael (2018), and in the western Pacific Ocean
255 during Hagupit (2008), Jangmi (2008), Fanapi (2010), and Malakas (2010). In addition, drifters
256 that are part of the Global Drifter Program⁵ array, often come close to tropical cyclones and
257 provide valuable SST and SLP observations. In the 2013-2018 period a total of 116 SVP and
258 SVPB drifters were located within 30 nm of the tracks of systems that eventually developed into
259 hurricanes (Centurioni et al., this issue). The effect of SLP drifter observation in improving TC
260 track forecast is, however, yet to be studied.

261 *Air deployed profiling instruments:* Airborne profiling instruments are often deployed in targeted
262 sampling mode in front of TCs in the Atlantic and Pacific basins. In the Atlantic, deployments of
263 Airborne eXpendables Bathythermographs (AXBTs), Airborne eXpendable Conductivity

⁴U.S. Glider Data Assembly Center: <https://gliders.ioos.us/data/>

⁵The Global Drifter Program: <http://www.aoml.noaa.gov/phod/gdp/index.php> and <http://gdp.ucsd.edu>

264 Temperature and Depth (AXCTDs) and Current Profilers (AXCPs) are generally conducted to
265 sample ocean conditions ahead and under TCs as part of the NOAA Hurricane Field Program
266 (Meyers et al., 2015; Jaimes et al., 2016; Zhang et al., 2018). Paired deployments of AXBTs and
267 dropsondes, for example, provide collocated measurements of SST, air temperature, humidity
268 and TC wind speed that allow for the estimation of bulk air-sea fluxes. Exchange coefficients
269 used in such computations are based on direct flux data (Zhang et al. 2008). These data provide
270 valuable information that is used to evaluate and improve TC model physics such as boundary-
271 layer parameterizations (e.g., Zhang et al., 2015). In recent years, the following Atlantic TCs
272 were sampled: Edouard (2014), Harvey (2017), Irma (2017), Maria (2017), Nate (2017), and
273 Michael (2018). In the Pacific, paired deployments of AXBTs and dropsondes were also carried
274 out during the 2010 Impact of Typhoon on Pacific (ITOP) international field experiment
275 (D'Asaro et al., 2014, see Section 3.6).

276 The more recent Air-Launched Autonomous Micro-Observer (ALAMO) (Jayne and Bogue,
277 2017) profiling float was also developed to be deployed from an aircraft Sonobuoy-A size tube
278 similarly to AXBTs (Sanabia et al., 2013). A key distinction between ALAMO floats and other
279 airborne expendable profiling instruments is that these floats are capable of sampling hundreds
280 of profiles continuously before, during, and after the passage of TCs for up to 6 months,
281 depending on instrument configurations. During the 2014-2018 period, a total of 60 ALAMO
282 floats were deployed in support of the NOAA Hurricane Field Program, in both the Atlantic and
283 eastern North Pacific basins.

284 *Profiling Floats:* Profiling floats (e.g., Riser et al., 2016) offer the advantage of providing a
285 sustained long-term and large-scale record of most of global oceans. Temperature and salinity
286 observations from Argo floats⁶ are routinely assimilated into operational ocean models (e.g.,
287 Chassignet et al., 2009) that are used to initialize the ocean component of hurricane forecast
288 models. In addition, operational Argo floats have been found to be very important in regions
289 where routine and/or opportunistic airborne AXBTs observations are lacking, e.g., in the case of
290 “Cat-6” supertyphoon Haiyan which devastated the Philippines in 2013 (Lin et al., 2014).

291 Profiling floats also offer valuable information of upper ocean processes contributing to EBCs
292 formation and intensification. Usual observation interval for Argo floats, however, is 10 days,
293 which is generally too long to capture the rapid air-sea interactions processes. High-frequency
294 and adaptive fine scale profiling float sampling are generally needed in order to fully capture
295 mesoscale ocean features usually associated with storm intensification, and also to characterize
296 the storm-induced upper ocean response in detail. Experimental high-frequency observations of
297 the upper 700 m with 6-hour interval were conducted using six Argo floats obtaining 73 profiles
298 under EBCs developed during the 2015/16 and 2016/17 winters. These data provided critical
299 information of ocean changes under EBCs in the Northwestern Pacific (Kuwano-Yoshida et al.,
300 2018), and emphasize the advantage of adaptive profiling float sampling using two-way

⁶Argo Global Data Assembly Center at: <http://www.usgodae.org/argo/argo.html>

301 communication systems over the traditional infrequent observations. In addition, new and
302 expanding coverage of Biogeochemical Argo float observations can also offer opportunities for
303 evaluating phytoplankton blooming in response to mixing forced by TCs and EBCs (e.g., Chacko
304 et al., 2017).

305 *EM-APEX (Electromagnetic Autonomous Profiling Explorer) floats* were developed to measure
306 the ocean temperature, salinity and current (and shear) during both weak and strong wind events.
307 The method was first developed in expendable current profilers deployed in hurricanes (Sanford
308 et al., 1987; Shay et al., 1992), in which the velocity measurements are based on motional
309 induction in that sea water moving through a magnetic field induces an electromagnetic force
310 that provides the two dimensional current field with depth (Sanford et al., 2007; 2011). EM-
311 APEX floats have been successfully air-deployed in front of hurricane Frances (2004), during the
312 ITOP missions in the western Pacific (2010) and more recently in Hurricane Michael (2018).
313 This type of float can profile to depths of 2000 m or over a specific depth region such as the
314 mixed layer through the seasonal thermocline. Mission profiles can be changed using iridium
315 remote sensing allowing for significant flexibility in an adaptive sample mode between the pre,
316 during and post missions for model initialization, air-sea interactions, and the oceanic response
317 for several weeks following passage. For example, during Hurricane Michael (2018), the profiler
318 sampled between 30-300 m during the storm at one hour intervals to assess the role of current
319 shear in vertical mixing processes to evaluate model parameterizations. That is, with the high
320 resolution measurements, the evolution of the Richardson numbers can be determined at vertical
321 resolution of 2-4 m in an active entrainment zone. In addition, the momentum flux from the
322 surface wind stress into the surface mixed layer provides a method to back out the surface drag
323 coefficient that are needed in examining the complex air-sea interactions that occur during
324 tropical cyclone passage (e.g., Shay and Brewster, 2010).

325 *Bio-logging* has also been used to collect in-situ meteorological and physical oceanographic
326 observations. Marine mammals (Campagna et al., 2000; Boehlert et al., 2001; Boyd et al., 2001),
327 seabirds (Koudil et al., 2000; Watanuki et al., 2001; Charrassin et al., 2002; Wilson et al., 2002),
328 sea turtles (Narazaki et al. 2009; Fukuoka et al., 2015) and fish (Block et al., 2001) have been
329 adopted as autonomous samplers of oceanographic parameters such as temperature, conductivity
330 and depth (Charrassin et al., 2002; Koudil et al., 2000; Watanuki et al., 2001; Wilson et al.,
331 2002; Block et al., 2001; Fedak, 2013). These animals often live around western boundary
332 currents and frontal systems where TCs and EBCs are often observed (Figure 4). In addition,
333 Bio-logging by sea turtles observed daily temperature profiles in surface layers in the
334 northwestern Pacific (Narazaki et al. 2009; Fukuoka et al. 2015). The profiles were collected
335 during 77 EBCs events in 6 consecutive winters. Both Argo floats and Bio-logging captured
336 rapid temperature changes under EBCs due to high-frequency observations. These ocean
337 observations are crucial to identify near-surface baroclinic zones and ocean-atmosphere fluxes of
338 heat and moisture. Such processes are crucial to the successful predictions and simulations of
339 EBCs.

340

341 **2.2 Ocean Parameters**

342

343 Some parameters estimated from both in situ and satellite observations have been
344 employed in TC and EBCs studies and forecasts, such as the TCHP/ OHC. The OHC, however,
345 has dimensional inequality with SST, it cannot be used in place of SST in the numerical models.
346 Besides, Price (2009), using an ocean model, argued that a depth-averaged temperature is a more
347 robust metric of hurricane-ocean interaction than is OHC. Hence, Ali et al. (2015) used the
348 satellite-derived OHC and D26 (depth of the 26 °C isotherm) to estimate ocean mean
349 temperature (OMT) using a few assumptions. This OMT is proved to have better predictability
350 for Indian monsoon rainfall compared to SST (Ali et al. 2015; Venugopal et al., 2018). Hence, it
351 is worthwhile to use OMT in place of SST in the numerical models and to assess the
352 improvement in forecasting the cyclones.

353 Thermodynamically, the subsurface ocean affects TCs through its control of TC-induced
354 cold SST wakes. When the cold wake is small (less than about 0.5°C), TCHP is a very good
355 predictor of TC intensification, exceeding the skill of other predictors such as SST and
356 vertically-averaged temperature (Figure 5; Balaguru et al., 2018). However, when the cold wake
357 is large, as can occur when SST is very warm and temperature stratification is shallow, ocean
358 dynamic temperature (Tdy) performs significantly better (Figure 5; Balaguru et al., 2018). Tdy is
359 defined as ocean temperature averaged from the surface to the post-storm mixed layer depth,
360 which depends on the upper-ocean stratification as well as the TC intensity and translation speed
361 (Balaguru et al., 2015). Furthermore, a serious limitation of temperature-based metrics such as
362 TCHP and OMT is that they do not account for salinity, which has shown to be important in all
363 TC basins (Wang et al., 2011; Balaguru et al., 2012b; Grodsky et al., 2012; Neetu et al., 2012;
364 Domingues et al., 2016; Foltz and Balaguru, 2016; Balaguru et al., 2016). The incorporation of
365 satellite-based sea surface salinity into Tdy, which explicitly includes salinity stratification, may
366 result in further improvements to statistical TC prediction schemes and enable more meaningful
367 validation of operational ocean analyses and forecasts.

368

369 **3. Highlighted Applications and Results**

370

371 In this section, key results, sampling strategies, and applications of ocean observations in
372 support of studies and forecasts of TCs and EBCs are described. These case studies provide
373 additional information on some of the successful examples of employing data derived from the
374 GOOS, new pilot networks, and targeted deployments to enhance our understanding of the
375 ocean-atmosphere interaction processes that can lead to TC and EBC intensification.

376

377

378 **3.1. The 2011 and 2012 Atlantic Hurricane Seasons: hurricanes Irene (2011) and Sandy**
379 **(2012).**

380 Over the broad continental shelf of the Middle Atlantic Bight along the US East Coast,
381 research carried out with gliders observations has identified and determined that a key ocean
382 feature characterized by cool subsurface waters (the “Cold Pool”; e.g., Houghton et al., 1982)
383 can be mixed with the surface waters under intense wind conditions, therefore impacting storm
384 intensity. Since this “Cold Pool” is not observable by satellites, in-situ observations, such as
385 those obtained by gliders are needed to capture its properties and impact on cyclone intensity
386 (Glenn et al., 2016; Seroka et al., 2016). For example, one glider deployed ahead of Hurricane
387 Irene (2011) observed larger than usual ahead-of-eye-center cooling of over 6°C (Seroka et al.,
388 2016) caused by intense mixing of surface waters with cold subsurface waters forced by the
389 hurricane winds. Subsequent ocean and atmosphere model sensitivity studies identified this
390 process as the missing component necessary to capture Irene rapid weakening just prior to
391 landfall. In contrast, glider observations collected during Hurricane Sandy (2012) showed that
392 the storm winds were downwelling favorable and led to offshore advection of the lower Cold
393 Pool waters, which prevented the upper ocean to cool, and likely favored the sustained intensity
394 of Sandy (Miles et al., 2015, 2017).

395

396 **3.2. The 2014 Atlantic Hurricane Season: Hurricanes Gonzalo (2014) and Fay (2014)**

397 Studies carried out using all ocean observations, including those from underwater gliders,
398 in the western tropical Atlantic and Caribbean Sea, were used to assess the pre and post ocean
399 conditions during hurricanes Fay and Gonzalo (2014). When Hurricane Gonzalo traveled north
400 of Puerto Rico, the general background ocean conditions were provided by Argo floats and
401 satellite-derived SST and SSH fields. In addition, there was one glider surveilling the upper
402 ocean temperature and salinity structure in the vicinity of the projected path of Gonzalo (Figure
403 6a). This glider provided the only observations that capture the presence of a 20 m thick barrier
404 layer (Domingues et al., 2015), a salinity stratified layer (e.g., Sprintall and Tomczak, 1992)
405 within the deeper isothermal layer. This layer inhibited vertical mixing and limited surface
406 cooling forced by Gonzalo’s winds to only 0.4°C, allowing the storm to intensify to Cat-4
407 (Domingues et al., 2015). When Gonzalo subsequently crossed the path of Fay near Bermuda
408 (Figure 6a), it weakened from Cat-3 to Cat-2 due to the upper ocean cooling of approximately
409 4°C observed in the wake of Fay (Goni et al., 2017).

410

411 **3.3. The 2017 Hurricane Season: Hurricanes Harvey, Irma, Jose, Maria, and Nate**
412

413 During the 2017 Atlantic hurricane season, underwater gliders, profiling floats, XBTs,
414 airborne observations, and other observing platforms collected crucial ocean data that served to

415 assess the upper ocean conditions and changes before, during, and after the passage of all
416 hurricanes. The 2017 Atlantic hurricane season was one of the most active in recent history with
417 17 named storms, and six major hurricanes. Here we describe ocean observations and key results
418 from hurricanes: Harvey, Irma, Maria, Jose, and Nate. Data from the ocean observing system
419 were used in support of operational hurricane intensity forecasts.

420 In August, Hurricane Harvey developed in the tropical Atlantic and travelled in the
421 Caribbean Sea south of Puerto Rico. In this area, observations from one underwater glider
422 showed that a relative shallow mixed layer favored cooling of the upper ocean, which together
423 with the moderate wind shear contributed to its lack of intensification in that region. Once it
424 reached the Gulf of Mexico, where Argo floats derived OHC were at a record level and SSTs
425 higher than 30 °C (Trenberth et al., 2018), Hurricane Harvey intensified from a tropical
426 depression (16 m s^{-1} / 56 km/h sustained winds) into a Cat-4 hurricane (59 m s^{-1} / 212 km/h
427 sustained winds) in less than 48 hours before making landfall.

428 In September, SST values of $\sim 30^\circ\text{C}$ were observed across the western Atlantic and
429 Caribbean (Figure 7), which along with low wind shear, helped sustain the development and
430 intensification of hurricanes Irma, Maria and Jose (Camp et al., 2018). Hurricane Irma, the
431 strongest TC globally in 2017, reached its maximum intensity (Cat-5) on September 6, while
432 traveling over waters north of Puerto Rico and Hispaniola. Underwater glider data showed that
433 the upper ocean conditions exhibited low salinity values at the surface, partially preventing the
434 upper ocean from mixing with the colder underlying waters, similar to Hurricane Gonzalo (2014;
435 Domingues et al., 2015, Dong et al., 2017). These observations also revealed that the upper 50 m
436 of the ocean cooled by approximately 1°C as a result of storm-induced mixing. Few days
437 following Irma, Hurricane Jose travelled off Puerto Rico, between 2-3 degrees in latitude to the
438 north of where Irma traveled. Its trajectory coincided at time with the cold wake left by
439 Hurricane Irma, experiencing, therefore, a relatively cooler and well mixed upper-ocean as
440 observed by underwater glider data. These cooler ocean conditions may have partly contributed
441 to its weakening from Cat-4 to 3. Later in the month, Hurricane Maria travelled in the Caribbean
442 Sea and later through the same approximate area as Irma in the tropical North Atlantic. On
443 September 20 and after entering the Caribbean Sea following a landfall in Dominica, Maria
444 peaked in intensity with maximum sustained winds of 78 m s^{-1} (280 km/h). Underwater glider
445 observations revealed the existence of a very stable barrier layer of approximately 30 m depth
446 along the path of Maria (Figure 8a), providing favorable ocean conditions for intensification. On
447 September 20, Maria made landfall in Puerto Rico as an intense Cat-4 hurricane. By the end of
448 September, positive SST anomalies recorded before the passage of these hurricanes had
449 dissipated due to the intense mixing caused by these major storms, and SSTs closer to neutral
450 conditions were observed. Farther north, Todd et al. (2018) used glider observations and volume
451 transport measurements in the Florida Straits to show that the Gulf Stream exhibited a large
452 freshwater anomaly that was attributable to rains from Irma and also a transient reduction in
453 volume transport that was attributable to winds forcing associated with the passing storms;

454 further studies with numerical simulations are needed to better understand the dynamics of the
455 storm impacts on the western boundary current.

456 In October, Hurricane Nate developed and steadily gained strength as travelling over
457 warm waters of the northwestern Caribbean Sea. Once Nate reached the Gulf of Mexico, EM-
458 APEX floats located in the proximity of the projected track (Figure 9) were reprogrammed to
459 sample rapidly every 2 to 4 hours intervals, and continuously measured vertical profiles of
460 temperature, salinity, current (including vertical shear), dissolved oxygen, chlorophyll
461 fluorescence, backscatter as proxy of particle concentration, and CDOM. In addition, one
462 hundred and forty AXCPs, and AXCTDs were deployed from the NOAA WP-3D aircraft prior,
463 during and after Nate (Figure 9). These observations showed the development of a velocity
464 response with magnitude of 0.5 to 0.75 m s⁻¹, with clear rotation of the current vector in the
465 upper ocean leading to strong current shear between 40 to 60 m depth. The development of
466 strong shear favored the deepening of the oceanic mixed layer under Nate by 10 to 15 m, and a
467 cooling of this layer of 1.5 to 2 °C. The observed response was predominantly near-inertial in
468 character, and likely impacted the air-sea fluxes and the intensity and structure of the storm (e.g.
469 Jaimes et al., 2016).

470

471 **3.4. Impact of Riverine Outflows on Atlantic Hurricanes**

472

473 Areas in the Caribbean Sea and Tropical North Atlantic, where hurricanes commonly
474 intensify, are sensitive to different freshwater sources, including major rivers such as the
475 Amazon and Orinoco (e.g., Kelly et al., 2000; Balaguru et al., 2012a; Johns et al., 2014) that can
476 contribute to barrier layer formations. These upper-ocean low salinity layers with enhanced
477 vertical density stratification close to the surface act as physical barriers to storm-induced
478 turbulent mixing, which may favor hurricane intensification by reducing the storm-induced SST
479 cooling, enabling continuous fluxes from the ocean into the hurricane. Barrier layers can be tens
480 of meters thick, and have been indicated as a potential contributor to the rapid intensification of
481 several TCs worldwide (e.g., Balaguru et al., 2012b).

482 Underwater glider observations revealed that major Atlantic hurricanes in 2017
483 experienced pre-existing barrier layer conditions along their trajectories (Figure 8a). Analysis of
484 satellite-derived chlorophyll data⁷ for August 2017 (Figure 8b) indicates that freshwater plumes
485 from the Amazon and Orinoco rivers were largely entrained by the circulation to areas where
486 these hurricanes travelled. In fact, historical chlorophyll data for the tropical North Atlantic
487 Ocean and Caribbean Sea (Figure 8c,d) indicates that entrainment of freshwater plumes from
488 these rivers in 2017 may have caused one of the largest freshwater transport events on record.
489 While investigation is still ongoing to assess the potential impact of these freshwater conditions
490 on the 2017 hurricanes, these results emphasize that the correct representation of salinity

⁷ NASA Ocean Color website: <https://oceancolor.gsfc.nasa.gov/>

491 conditions within coupled TC forecast models can be key to produce accurate hurricane
492 predictions. This may be especially true for areas that are particularly sensitive to large
493 freshwater sources, such as the Caribbean Sea, Gulf of Mexico, and tropical North Atlantic
494 Ocean.

495

496 **3.5. Development of Bio-Logging as an ocean observation platform for EBCs**

497

498 Flight and drift paths and of sea birds soaring and floating over the ocean surface enable
499 measurement of fine-scale winds and currents. Yonehara et al. (2016) and Goto et al. (2017)
500 found out that fine-scale flight trajectories by recording one position per second provide 5-min to
501 1-hour interval surface wind direction and speed along the trajectories. The bird-estimated wind
502 directions showed good agreement with those from satellite, although wind speeds were slower
503 than satellite winds because sea birds flew at lower altitudes than 10 m at which satellite winds
504 were calibrated. Only the wind estimates from three birds had meaningful impact on data
505 assimilation when severe rainfall occurred in Japan associated with two typhoons using regional
506 numerical forecast system (Wada et al., 2017). Yoda et al. (2014) developed a new method for
507 obtaining in-situ ocean current measurements by using sea birds with GPS/GNSS loggers
508 floating at the surface as Lagrangian current sensors akin to drifting buoys. The sea birds forage
509 boundary areas between two oceanic mesoscale eddies and their edges where primary
510 productivity and prey density are thought to be high. The current data from sea birds improved
511 reproducibility of eddies through data assimilation into an operational ocean nowcast/forecast
512 system (Miyazawa et al., 2015).

513

514 **3.6. The 2010 ITOP field campaign**

515

516 The ITOP international field campaign in the western North Pacific Ocean is an important
517 example for future field observation strategy and planning (Figure 10; D'Asaro et al., 2014). The
518 western North Pacific was chosen because this basin is where the largest number and the most
519 intense TCs are usually recorded (Figure 1). In the summer of 2010, the ITOP field campaign
520 used targeted aircraft AXBT observations to collect the pre-storm temperature profiles ahead of
521 3 TCs of distinct intensity: Megi, Fanapi, and Malakas. Supertyphoon Megi (with peak intensity
522 $82 \text{ m s}^{-1}/296 \text{ km/h}$, Cat-5) was the most intense TC recorded globally until 2010, while Fanapi
523 was a Cat-3 moderate TC and Malakas was a Cat-2 TC. The pre-TC ocean conditions were
524 different among these three TCs (Figure 11a). Among the three, Megi intensified over warm
525 ocean conditions temperatures, characterized by TCHP values larger than 140 kJ cm^{-2} , and D26
526 of 120 m. In contrast, both Fanapi and Malakas travelled over waters with shallower D26, with
527 TCHP values lower than 100 kJ cm^{-2} . Analysis of the available ocean observations revealed that
528 these large differences in upper ocean heat content may have played a key role in the
529 intensification of these TCs (Lin et al., 2013a; D'Asaro et al., 2014).

530 In addition to assessing the pre-TC ocean conditions using AXBT profile observations, the
531 collection of ocean-atmosphere paired observations during TC intensification were also carried
532 out. These observations were collected to evaluate actual air-sea sensible and latent heat fluxes.
533 The correct representation of these fluxes is needed in order to obtain accurate TC intensification
534 forecasts, since air-sea fluxes are the actual energy that will lead to TC intensification. Direct
535 observations of air-sea fluxes were obtained employing co-incident/co-located pair atmospheric
536 dropsonde and ocean AXBT in TC-penetration flights (see Figure 11c). With these unique
537 observations obtained during ITOP, accurate air-sea sensible and latent fluxes were obtained
538 (Lin et al., 2013a; D'Asaro et al., 2014), and revealed that enthalpy fluxes were substantially
539 larger during Supertyphoon Megi as it reached Cat-2 (Figure 11c), enabling Megi to continue
540 intensifying until it became a Cat-5 Supertyphoon. These results obtained during ITOP
541 emphasize the value of paired, co-located, ocean-atmosphere observations to improve model
542 prediction performance, and for improving our understanding on the role that different types of
543 ocean conditions can play in the TC intensification processes.

544

545

546 **4. Impact of Ocean Data in Tropical Cyclone Intensity Forecasts**

547 A variety of observations collected near TCs in recent years have had demonstrated
548 impacts on the fidelity of TCs forecasts, typically by reducing errors and biases in analyses used
549 to initialize the ocean component of coupled prediction models. For example, Halliwell et al.
550 (2011) analyzed the impact of multiple factors toward reducing errors in ocean analyses in the
551 Gulf of Mexico prior to Hurricane Isaac (2005) produced by the HYbrid-Coordinate Ocean
552 Model (HYCOM). They determined that assimilation of ocean observations is a leading-order
553 factor in reducing initialization errors in comparison to ocean model attributes such as vertical
554 mixing and surface flux parameterizations, along with model resolution.

555 More recently, Dong et al. (2017) conducted observing system experiments (OSE) focused
556 on the influence of conventional ocean observing systems plus underwater glider data on
557 prediction of Gonzalo's intensity. A twin experiment was performed comparing an analysis that
558 assimilated underwater glider data from July 15 to October 13 along with other in-situ and
559 satellite observations to an analysis produced by an unconstrained model simulation. These two
560 analyses were then used to initialize the high-resolution Hurricane Weather Research and
561 Forecasting (HWRf)-HYCOM coupled forecast system (Dong et al., 2017). Assimilation of
562 subsurface observations from gliders improved the representation of pre-storm vertical structure
563 of both temperature (Figure 6b) and salinity, capturing the barrier layer previously observed in
564 the region (Domingues et al, 2016). Consequently, forecast intensity errors (e.g., Figure 6c) were
565 reduced by approximately 50% as a result of assimilating all available observations, enabling a
566 substantially improved forecast for Hurricane Gonzalo.

567 OSEs are now being conducted for the 2017 North Atlantic hurricane season. The fields of
568 mean TCHP and D26 presented in Figure 12 demonstrate the impact of assimilating all ocean

569 profilers (Argo and Alamo floats plus underwater gliders). Comparing fields produced by an
570 unconstrained model simulation (Figures 12c and 12d) to observation-based estimates provided
571 by the AOML/PhOD TCHP analysis product (Figures 12a and 12b), the unconstrained model
572 produces TCHP that is too small and an upper-ocean warm layer that is too thin across the entire
573 North Atlantic hurricane development region. Assimilation of all ocean profilers (Figures 12e
574 and 12f) substantially corrects these large-scale biases. The planned next step in this analysis will
575 be to assess the impact on intensity prediction by using these fields to initialize the HYCOM-
576 HWRF prediction model.

577 Observing System Simulation Experiments (OSSEs) have also been performed over the
578 North Atlantic hurricane region. Given that the Nature Run, a validated, unconstrained, and
579 realistic ocean simulation by a state-of-the-art ocean model, is known, it is possible to evaluate
580 new observing systems and alternate deployment strategies for existing systems. Previous OSSEs
581 have quantitatively assessed the positive impacts of existing observing systems and different
582 deployment strategies for systems, such as underwater gliders and picket-fence deployments of
583 thermistor chains (Halliwell et al., 2017a), and also for pre-storm airborne ocean profiler surveys
584 (Halliwell et al., 2017b). More recently, OSSEs were performed to demonstrate the advantages
585 of collecting ocean profiles from moving platforms such as gliders compared to collecting
586 profiles from stationary platforms. These results are summarized in another OceanObs White
587 Paper (Fujii et al., this issue). Moving forward, OSSEs will continue to be an important tool for
588 the design and implementation of optimized ocean sampling strategies in support of both TCs
589 and EBCs forecasts, while OSEs will also continue providing further quantitative information on
590 the impacts of different components of the ocean observing system.

591

592 **5. Data Management**

593

594 Efficient data management, including data transmission is critical for ensuring
595 observations are available in real-time or near-real-time for assimilation into forecast models.
596 Latency in data availability can have unwanted downstream effects on the use of observations
597 within operational models.

598

599 For weather forecast purposes, it is critical that Data Assembly Centers (DACs) and
600 operators transmit the data in real time to systems such as the Global Telecommunications
601 System (GTS) for assimilation into numerical forecast models to ensure increased data
602 availability for forecasters and to validate models. In order to make the data available for
603 assimilation into forecast numerical models, most of the data obtained by the different
604 observational platforms considered here need to be transmitted in real-time or near-real time
605 through different satellite networks. After its reception on land the data is submitted in most
606 cases to quality analysis (QA) and quality control (QC) procedures which are typically platform
607 dependent and are designed to identify possible inaccuracies in the observations. For most

608 platforms these QC procedures include test designed to identify data gaps or missing values,
609 spikes or unrealistic gradients in the data, invalid dates or locations, among other error sources.
610 As a result, the data is normally not modified at this step, but individual records are flagged
611 according to the results of the tests applied, or the data from a malfunctioning platform may be
612 blacklisted and removed altogether from GTS distribution. The data is then encoded into
613 different traditional alphanumeric formats (for example, FM 63-XI Ext. BATHY for XBTs and
614 AXBTs, FM 64-XI Ext. TESAC for Argo floats and underwater gliders; World Meteorological
615 Organization, 2015a - Part A), or into binary universal form for the representation of
616 meteorological data (FM 94-XIV BUFR, World Meteorological Organization, 2015a - Part B).
617 For example, the drifting buoys format TM315009 is used by the data processing Center of the
618 Lagrangian Drifter Laboratory at the Scripps Institution of Oceanography, by MeteoFrance and
619 the UK Met Office for the ESURFMAR contribution to the Global Surface Drifter Array and
620 submitted into the GTS (World Meteorological Organization, 2015b) for near real-time
621 distribution and numerical model assimilation. Additionally, these data are submitted into data
622 centers such as the Global Temperature and Salinity Profile Programme (GTSPP; XBT, Argo
623 floats, underwater glider), the U.S. IOOS underwater gliders Data Assembly Center (DAC),
624 NOAA/NCEI (XBT, Argo, underwater glider) as part of long term archival and for distribution
625 for other delayed-mode scientific applications. At this step the data may be submitted to delayed-
626 mode QC that may result in flags for individual records or in modifications to the data set, in
627 order to ensure the highest possible data quality for all applications.

628
629 For research and retrospective analysis, data management is important to ensuring
630 collected observations from various platforms, operated by diverse organizations, is easily
631 available, QA/QCed, and compatible with relevant standards. DACs can be leveraged to provide
632 a diverse observation platform community a single place to store, share, archive, and quality
633 control their data. In addition to providing standardized, easy to access, QA/QCed ocean
634 observations critical for extreme weather events.

635

636 **6. The vision for the next 10 years**

637 **6.1 Ocean observations in support of tropical cyclones studies and forecasts**

638 A dedicated integrated multiplatform ocean observing system in support of studies and
639 forecasts of TCs is not currently in place. Analysis of ocean observations from the largely
640 climate-focused ocean observing system may often provide valuable information on the
641 mechanisms and processes associated with these extreme weather conditions. Ocean data in
642 support of extreme weather events need to focus on resolving mesoscale features, barrier layers,
643 spatial variability of warm current jets, mesoscale ocean heat content changes, surface waves
644 (Centurioni et al., this issue), etc. prior and during the season in each basin where TC occur, with
645 distribution of data in real-time. However, the scientific and operational requirements of
646 observing platforms, such as profiling floats, moorings (Foltz et al., this issue; Masumoto et al.

647 this issue; Smith et al., this issue), expandable probes (Goni et al, this issue), etc. do not support
648 these requirements. Sustained and targeted, high resolution ocean observations provide a means
649 to better understand the processes responsible for the rapid evolution of the ocean and its
650 feedback on the atmosphere during these extreme weather conditions. These concerns have been
651 presented and discussed in workshops on TCs from a global perspective, as for example where
652 WMO Recommendations focused on structure and intensity of TCs (Shay et al., 2014).

653 Pilot networks of sustained multi-platform observations and targeted observations in the
654 tropical Atlantic during hurricane season, which allow proper representation of the upper ocean
655 density field in areas where TC intensification and weakening may occur, have proven to provide
656 key upper ocean observations to initialize numerical ocean-atmosphere coupled forecast models.
657 Assimilation of oceanic observations on intensity forecast errors has been quantitatively assessed
658 for Hurricane Gonzalo (2014), where glider data improved the representation of the ocean
659 component of the ocean-atmosphere coupled forecast model and, together with standard ocean
660 observations (SSH from altimetry, SST from satellite radiometers, temperature and salinity from
661 profiling floats), reduced intensity forecast errors for Hurricane Gonzalo by almost 50% in the
662 HYCOM-HWRF numerical model. OSEs similar to the work by Dong et al. (2017), studying the
663 impact of the assimilation of ocean observations on hurricane prediction, need to be extended to
664 more storms in order to provide a more robust estimate of the benefit of various types of
665 observations. These experiments should ideally be performed using operational models, in order
666 to quantify the benefit of ocean observations in operational conditions. Furthermore, the OSSE
667 approach dedicated to hurricanes should continue to be followed in order to optimize the
668 deployment of dedicated TC ocean observations, typically gliders and airborne profilers.

669 For the next decade, coupled model system will extend to multi-way dynamic coupling. In
670 recent years, EMC has demonstrated 3-way dynamic coupling with HYCOM-WaveWatchIII-
671 HWRF model. This poses not only revisiting air-sea interaction dynamics but also exploring
672 observational measurements to support research and simulations. The importance of air-sea flux
673 exchanges to the TC development is widely known, and yet simulations are still based on the
674 bulk parameterizations. In order to support the evolving modeling efforts, observational effort
675 should accordingly extend to collecting data on waves, sea sprays, roughness, turbulence, and
676 relative humidity over the ocean.

677 Sustained and targeted observations carried out in locations where TCs often intensify in
678 the warm tropics or boundary currents and rapidly weaken on mid latitude continental shelves
679 provide one of the best strategies in support of hurricane studies and forecasts. Underwater
680 gliders and other autonomous vehicles offer one option for carrying out sustained surveillance in
681 support of TCs studies and forecasts, given that these vehicles can be remotely operated along
682 predetermined routes, provide observations in real-time continuously for several months, and can
683 withstand hurricane-force winds. Targeted and rapid response observations also provide critical
684 information that instruments surveying on sustained mode cannot. For instance, air-deployed
685 instrumentation are particularly useful since they are deployed from aircrafts already tasked with

686 storm surveillance, they are logistically easier to position along the forecast track ahead of a TC.
687 Flexible deployments of in-situ marine and airborne platforms allow for co-located
688 measurements with other air/ocean observing systems which are key for advancing science of
689 understanding air-sea flux interactions across the oceanic surface. These can also help provide
690 precious data points for future coupled data assimilation methods under active consideration for
691 balanced initialization of next generation coupled hurricane models.

692 With respect to satellite observations, with the advent of wide swath, high resolution
693 altimetry (e.g., Fu and Ubelmann, 2014), it is expected that the ocean background information, in
694 particular the surface characteristics of features that can intensify or weaken cyclones, will be
695 able to provide more detailed information for analysis and data for assimilation into forecast
696 models. High-resolution swath altimetry data will also enable the evaluation of air-sea
697 interaction processes during high-wind events in detail, such as, for example, the generation of
698 internal waves in the wake of TCs. Satellite measurements of surface salinity have potential for
699 improving our understanding of the oceanic factors and processes that lead to TC intensification,
700 especially in the western Atlantic and Bay of Bengal, where there is persistent shallow salinity
701 stratification. It is important that these measurements continue, along with satellite SST, sea
702 level, and winds. Temperature and salinity profiles from Argo are also crucial for relating
703 satellite surface measurements to subsurface conditions.

704 Considering the positive impacts of upper-ocean observations from pilot networks, and
705 targeted deployments, the following key recommendations have been identified to continue and
706 enhance ocean observations in support of TCs:

- 707 ▪ Maintain the elements of the observing system that have proven to valuable for Tropical
708 Cyclone ocean research and operational intensity forecast.
- 709 ▪ Utilize numerical Observing System Experiments to quantify the impact of the current
710 ocean observing platforms in Tropical Cyclone forecasts.
- 711 ▪ Evaluate optimal observational strategies in support of Tropical Cyclone studies and
712 forecasts using numerical Observing System Simulation Experiments.
- 713 ▪ Implement sustained and targeted pilot observations (gliders, profiling floats, drifters, etc)
714 dedicated to improve Tropical Cyclone intensity forecasts; and foster co-incident, co-located
715 paired air-deployed profile observations (AXBTs, AXCTDs, floats, thermistor chains, etc.)
716 of ocean temperature, salinity, and currents.
- 717 ▪ Foster additional sustained measurements of sea level pressure (e.g., from drifters and
718 moorings), and of waves, sea spray, and mixed-layer turbulence to help develop, evaluate,
719 and validate boundary layer parameterizations (e.g., from gliders).
- 720 ▪ Use upper ocean metrics (e.g. Tropical Cyclone Heat Potential, ocean mean temperature,
721 barrier layer thickness, etc) derived from profile and satellite ocean observations in the
722 operational evaluation and validation of numerical forecast models.

- 723 ▪ Continue with efforts focused on improving coupled ocean-atmospheric numerical weather
724 models, especially those relating to enhancing ocean data assimilation techniques and mixed
725 layer parametrizations.
- 726 ▪ Create an ocean database easily accessible to the scientific community to facilitate research
727 in support of assessments of the role of the ocean in Tropical Cyclones studies.
- 728 ▪ Enhance data management efforts to transmit and QA/QC data in real-time for assimilation
729 in operational forecast models.

730

731 **6.2 Ocean observations in support of extratropical bomb cyclones studies**

732 The recommended observations to improve the understanding of ocean-atmosphere interactions
733 during EBC events are:

- 734 ▪ Increase efforts to implement and improve coverage of high-frequency and high-resolution
735 observations using profiling instruments and Bio-logging to detect oceanic fronts associated
736 with western boundary currents in winter in support of Extratropical Bomb Cyclones
737 studies.
- 738 ▪ Enhance efforts dedicated to observing surface wind, and waves, using surface drifters, and
739 floating seabirds equipped with weather and motion sensors, respectively, to estimate air-sea
740 flux exchanges under Extratropical Bomb Cyclones.
- 741 ▪ Foster additional efforts aimed at observing ocean turbulent mixing induced by
742 Extratropical Bomb Cyclones using, profiling floats and other platforms (e.g. gliders,
743 moorings, etc).
- 744 ▪ Incorporate real-time meteo-ocean observations, including ocean bottom pressure, in
745 moorings from the Tsunami monitoring network in support of Extratropical Bomb Cyclones
746 studies and forecasts.

747 The loggerhead turtles favor over 15°C, which is corresponded to northern edges of the
748 Kuroshio and its extension near the surface in winter. A feasibility study for data assimilation of
749 temperature measurements by the turtles suggests that the turtle measurements captured the
750 warm core rings separating from the Kuroshio Extension better than the Oyashio intrusion
751 branches (Miyazawa et al., in review). Observation interval and depth of modern Argo floats can
752 be controlled using two-way satellite communication. Interactive operation of the floats with
753 satellite and assimilated data will enable high-frequency and high-resolution observation at
754 fronts, i.e. the floats observe short interval if satellite and assimilated data suggest that the floats
755 are located near the SST fronts. The in-situ observations will complement satellite observations,
756 increase temporal sampling, and enable resolving the fine structure associated with SST fronts.

757 Air-sea interaction under EBCs is one of the most unclear processes because of few in-situ
758 observations and lack of satellite observations by thick clouds and heavy rain. Seabirds are often

759 observed to fly and float under EBCs to forage (Yoda et al., 2014; Yonehara et al., 2016; Goto et
760 al., 2017), providing an additional potential source of environmental data. Estimation of surface
761 winds and waves using Bio-logging GNSS and motion sensor can provide useful information
762 about air-sea interaction processes under EBCs as well as their temperature and pressure
763 measurements. In addition, the development of profiling floats equipped with motion sensors can
764 also help to provide metrics to evaluate ocean mixing near the sea surface.

765 To monitor Tsunami, several real-time observation networks of ocean bottom pressure
766 have been established (Kaneda, 2010; Bernard and Meinig, 2011; Lawson et al., 2011;
767 Mochizuki et al., 2017). Most of sites in the networks are located under the area where EBCs
768 frequently develop. Recently, seismic stations on land can catch microseisms induced by EBCs
769 (Nishida and Takagi, 2016). The real-time monitoring networks will provide oceanic responses
770 to EBCs and information of winds and waves which may contribute to forecast improvement of
771 EBCs.

772

773 **7. Summary**

774 In this community white paper, a summary of current ocean observing efforts, and recent
775 research findings in support of studies and forecasts of TCs and EBCs is provided. Substantial
776 progress has been accomplished over the past decade in terms of ocean observations, of
777 improving the knowledge that the ocean plays on TCs and EBCs, and of implementing state-of-
778 the art coupled forecast models into operational mode. These advances have largely addressed
779 previous recommendations raised by the scientific community during OceanObs' 09 (e.g. Goni et
780 al., 2010), and emphasize the critical value of sustained and targeted ocean observations, real-
781 time data transmission, and of multi-platform efforts.

782 With recent advances in ocean modelling, and on coupling atmospheric-ocean models,
783 operational forecasts increasingly rely more on assimilating real-time data of ocean conditions to
784 produce accurate ocean, weather and extreme weather forecasts. Assimilation of ocean
785 observations can largely help improve hurricane intensity forecasts (e.g. Dong et al., 2017), for
786 example, and in all regions, OSEs can assist in quantifying the impact of upper ocean
787 observations on TC and EBCs forecasts. Similarly, OSSEs can also be applied to various regions
788 to design optimal and most cost-effective deployment strategies for both targeted and sustained
789 observations in support of EBCs and TCs.

790 Given the large benefits provided by the ocean observing system in support of extreme
791 weather studies and forecasts, it is expected that current components are maintained and possibly
792 expanded over the next decade. In addition, new technologies, pilot networks, and targeted
793 deployments are greatly expanding the observation capabilities of the current ocean observing
794 system, and incorporating these components into a sustained mode of observation could likely
795 considerably improve current capabilities. Finally, considering the large number of countries

796 whose coastal areas are often impacted by TCs and EBCs, results and advances presented here
797 emphasize the critical value of carrying out a coordinated international effort in the design,
798 implementation, maintenance, and data management of key aspects of ocean observations that
799 will ensure the feasibility of logistical, operational, and research activities.

800

801 **References**

802

803 Ali, M. M., Jagadeesh, P. S. V., and Jain, S. (2007). Effects of eddies on Bay of Bengal cyclone
804 intensity. *Eos Trans. Am. Geophys. Union* 88, 93–95. doi:10.1029/2007EO080001.

805 Ali, M. M., Kashyap, T., and Nagamani, P. V. (2013). Use of sea surface temperature for
806 cyclone intensity prediction needs a relook. *Eos Trans. Am. Geophys. Union* 94, 177–177.
807 doi:10.1002/2013EO190005.

808 Ali, M. M., Nagamani, P. V., Sharma, N., Gopal, R. T. V., Rajeevan, M., Goni, G. J., et al.
809 (2015). Relationship between ocean mean temperatures and Indian summer monsoon
810 rainfall. *Atmospheric Sci. Lett.* 16, 408–413. doi:10.1002/asl2.576.

811 Balaguru, K., Chang, P., Saravanan, R., and Jang, C. J. (2012a). The barrier layer of the Atlantic
812 warm pool: formation mechanism and influence on the mean climate. *Tellus Dyn. Meteorol.*
813 *Oceanogr.* 64, 18162.

814 Balaguru, K., Chang, P., Saravanan, R., Leung, L. R., Xu, Z., Li, M., et al. (2012b). Ocean
815 barrier layers' effect on tropical cyclone intensification. *Proc. Natl. Acad. Sci.* 109, 14343–
816 14347. doi:10.1073/pnas.1201364109.

817 Balaguru, K., Foltz, G. R., Leung, L. R., Asaro, E. D., Emanuel, K. A., Liu, H., et al. (2015).
818 Dynamic potential intensity: An improved representation of the ocean's impact on tropical
819 cyclones. *Geophys. Res. Lett.* 42, 6739–6746. doi:10.1002/2015GL064822.

820 Balaguru, K., Foltz, G. R., Leung, L. R., and Emanuel, K. A. (2016). Global warming-induced
821 upper-ocean freshening and the intensification of super typhoons. *Nat. Commun.* 7, 13670.
822 doi:10.1038/ncomms13670.

823 Balaguru, K., Foltz, G. R., Leung, L. R., Hagos, S. M., and Judi, D. R. (2018). On the use of
824 ocean dynamic temperature for hurricane intensity forecasting. *Weather Forecast.* 33, 411–
825 418. doi:10.1175/WAF-D-17-0143.1.

826 Bernard, E. N., and Meinig, C. (2011). "History and future of deep-ocean tsunami
827 measurements," in *OCEANS' 11 MTS/IEEE*, Kona, Japan.
828 doi:10.23919/OCEANS.2011.6106894.

829 Block, B. A., Dewar, H., Blackwell, S. B., Williams, T. D., Prince, E. D., Farwell, C. J., et al.
830 (2001). Migratory movements, depth preferences, and thermal biology of Atlantic bluefin
831 tuna. *Science* 293, 1310–1314. doi:10.1126/science.1061197.

- 832 Boehlert, G. W., Costa, D. P., Crocker, D. E., Green, P., O'Brien, T., Levitus, S., et al. (2001).
 833 Autonomous pinniped environmental samplers: using instrumented animals as
 834 oceanographic data collectors. *J. Atmospheric Ocean. Technol.* 18, 1882–1893.
 835 doi:10.1175/1520-0426(2001)018<1882:APESUI>2.0.CO;2.
- 836 Booth, J. F., Thompson, L., Patoux, J., and Kelly, K. A. (2012). Sensitivity of midlatitude storm
 837 intensification to perturbations in the sea surface temperature near the Gulf Stream. *Mon.*
 838 *Weather Rev.* 140, 1241–1256. doi:10.1175/MWR-D-11-00195.1.
- 839 Boyd, I. L., Hawker, E. J., Brandon, M. A., and Staniland, I. J. (2001). Measurement of ocean
 840 temperatures using instruments carried by Antarctic fur seals. *J. Mar. Syst.* 27, 277–288.
 841 doi:10.1016/S0924-7963(00)00073-7.
- 842 Camp, J., Scaife, A. A., and Heming, J. (2018). Predictability of the 2017 North Atlantic
 843 hurricane season. *Atmospheric Sci. Lett.* 19, e813. doi:10.1002/asl.813.
- 844 Campagna, C., Rivas, A. L., and Marin, M. R. (2000). Temperature and depth profiles recorded
 845 during dives of elephant seals reflect distinct ocean environments. *J. Mar. Syst.* 24, 299–
 846 312. doi:10.1016/S0924-7963(99)00091-3.
- 847 Catto, J. L., Shaffrey, L. C., and Hodges, K. I. (2010). Can climate models capture the structure
 848 of extratropical cyclones? *J. Clim.* 23, 1621–1635. doi:10.1175/2009JCLI3318.1.
- 849 Centurioni, L., Braasch, L., Lauro, E. D., Contestabile, P., Leo, F. D., Casotti, R., et al. (2016).
 850 “A new strategic wave measurement station off Naples port main breakwater,” in *Coastal*
 851 *Engineering Proceedings*, 36. doi:10.9753/icce.v35.waves.36.
- 852 Centurioni, L., Horányi, A., Cardinali, C., Charpentier, E., and Lumpkin, R. (2017). A global
 853 ocean observing system for measuring sea level atmospheric pressure: Effects and impacts
 854 on numerical weather prediction. *Bull. Am. Meteorol. Soc.* 98, 231–238.
- 855 Centurioni, L. R. (2010). Observations of large-amplitude nonlinear internal waves from a
 856 drifting array: Instruments and methods. *J. Atmospheric Ocean. Technol.* 27, 1711–1731.
- 857 Centurioni, L. R., Turton, J., Lumpkin, R., Braasch, L. J., Brassington, G., Chao, Y., et al. (this
 858 issue). Multidisciplinary Global In-Situ Observations of Essential Climate and Ocean
 859 Variables at the Air-Sea Interface in Support of Climate Variability and Change Studies and
 860 to Improve Weather Forecasting, Pollution, Hazard and Maritime Safety Assessments.
 861 *Front. Mar. Sci.*
- 862 Chacko, N. (2017). Chlorophyll bloom in response to tropical cyclone Hudhud in the Bay of
 863 Bengal: Bio-Argo subsurface observations. *Deep Sea Res. Part Oceanogr. Res. Pap.* 124,
 864 66–72. doi:10.1016/j.dsr.2017.04.010.
- 865 Chang, E. K. (2017). Projected significant increase in the number of extreme extratropical
 866 cyclones in the Southern Hemisphere. *J. Clim.* 30, 4915–4935.
- 867 Charrassin, J.-B., Park, Y.-H., Maho, Y. L., and Bost, C.-A. (2002). Penguins as
 868 oceanographers unravel hidden mechanisms of marine productivity. *Ecol. Lett.* 5, 317–319.
 869 doi:10.1046/j.1461-0248.2002.00341.x.

- 870 Chassignet, E. P., Hurlburt, H. E., Metzger, E. J., Smedstad, O. M., Cummings, J. A., Halliwell,
871 G. R., et al. (2009). US GODAE: global ocean prediction with the HYbrid Coordinate
872 Ocean Model (HYCOM). *Oceanography* 22, 64–75.
- 873 Colle, B. A., Booth, J. F., and Chang, E. K. (2015). A review of historical and future changes of
874 extratropical cyclones and associated impacts along the US East Coast. *Curr. Clim. Change*
875 *Rep.* 1, 125–143.
- 876 D’Asaro, E. A., Black, P. G., Centurioni, L. R., Chang, Y.-T., Chen, S. S., Foster, R. C., et al.
877 (2014). Impact of typhoons on the ocean in the Pacific. *Bull. Am. Meteorol. Soc.* 95, 1405–
878 1418.
- 879 DeMaria, M., and Kaplan, J. (1994). A statistical hurricane intensity prediction scheme (SHIPS)
880 for the Atlantic basin. *Weather Forecast.* 9, 209–220.
- 881 DeMaria, M., Knaff, J. A., and Sampson, C. (2007). Evaluation of long-term trends in tropical
882 cyclone intensity forecasts. *Meteorol. Atmospheric Phys.* 97, 19–28.
- 883 DeMaria, M., Mainelli, M., Shay, L. K., Knaff, J. A., and Kaplan, J. (2005). Further
884 improvements to the statistical hurricane intensity prediction scheme (SHIPS). *Weather*
885 *Forecast.* 20, 531–543.
- 886 DeMaria, M., Sampson, C. R., Knaff, J. A., and Musgrave, K. D. (2014). Is tropical cyclone
887 intensity guidance improving? *Bull. Am. Meteorol. Soc.* 95, 387–398.
- 888 Domingues, R., Goni, G., Bringas, F., Lee, S.-K., Kim, H.-S., Halliwell, G., et al. (2015). Upper
889 ocean response to Hurricane Gonzalo (2014): Salinity effects revealed by targeted and
890 sustained underwater glider observations. *Geophys. Res. Lett.* 42, 7131–7138.
- 891 Dong, J., Domingues, R., Goni, G., Halliwell, G., Kim, H.-S., Lee, S.-K., et al. (2017). Impact
892 of assimilating underwater glider data on Hurricane Gonzalo (2014) forecasts. *Weather*
893 *Forecast.* 32, 1143–1159.
- 894 Elsner, J. B., Kossin, J. P., and Jagger, T. H. (2008). The increasing intensity of the strongest
895 tropical cyclones. *Nature* 455, 92–95. doi:10.1038/nature07234.
- 896 Emanuel, K. (2015). Effect of upper-ocean evolution on projected trends in tropical cyclone
897 activity. *J. Clim.* 28, 8165–8170.
- 898 Fedak, M. A. (2013). The impact of animal platforms on polar ocean observation. *Deep Sea*
899 *Res. Part II Top. Stud. Oceanogr.* 88–89, 7–13. doi:10.1016/j.dsr2.2012.07.007.
- 900 Foltz, G. R., Brandt, P., Rodriguez-Fonseca, M., Hernandez, F., Dengler, M., Rodrigues, R., et
901 al. (this issue). The Tropical Atlantic Observing System. *Front. Mar. Sci.*
- 902 Foltz, G. R., and Balaguru, K. (2016). Prolonged El Niño conditions in 2014-2015 and the rapid
903 intensification of Hurricane Patricia in the eastern Pacific: El Niño and Hurricane Patricia.
904 *Geophys. Res. Lett.* 43, 10,347-10,355. doi:10.1002/2016GL070274.

- 905 Fu, L.-L., and Ubelmann, C. (2014). On the transition from profile altimeter to swath altimeter
906 for Observing Global Ocean Surface Topography. *J. Atmospheric Ocean. Technol.* 31, 560–
907 568. doi:10.1175/JTECH-D-13-00109.1.
- 908 Fujii, Y., Remy, E., Zuo, H., Oke, P., Halliwell, G., Garparin, F., et al. (this issue). Observing
909 system evaluation based on ocean data assimilation and prediction systems: On-going
910 challenges and future vision for designing/supporting ocean observational networks. *Front.*
911 *Mar. Sci.*
- 912 Fukuoka, T., Narazaki, T., and Sato, K. (2015). Summer-restricted migration of green turtles
913 *Chelonia mydas* to a temperate habitat of the northwest Pacific Ocean. *Endanger. Species*
914 *Res.* 28, 1–10.
- 915 Glenn, S. M., Miles, T. N., Seroka, G. N., Xu, Y., Forney, R. K., Yu, F., et al. (2016). Stratified
916 coastal ocean interactions with tropical cyclones. *Nat. Commun.* 7.
917 doi:10.1038/ncomms10887.
- 918 Goni, G., Sprintall, J., Bringas, F., Cheng, L., Cirano, M., Dong, S., et al. (this issue). More than
919 50 years of successful continuous temperature section measurements by the Global
920 Expendable Bathythermograph Network, its integrability, societal benefits, and future.
921 *Front. Mar. Sci.*
- 922 Goni, G., DeMaria, M., Knaff, J., Sampson, C., Ginis, I., Bringas, F., et al. (2009). Applications
923 of satellite-derived ocean measurements to tropical cyclone intensity forecasting.
924 *Oceanography* 22, 190–197.
- 925 Goni, G., DeMaria, M., Knaff, J., Sampson, C., Price, J., Mehra, A., et al. (2010). “The ocean
926 observing system for tropical cyclone intensification forecasts and studies,” in *OceanObs’*
927 *09 Conference*, Venice, Italy.
- 928 Goni, G. J., Todd, R. E., Jayne, S. R., Halliwell, G., Glenn, S., Dong, J., et al. (2017).
929 Autonomous and Lagrangian ocean observations for Atlantic tropical cyclone studies and
930 forecasts. *Oceanography* 30, 92–103.
- 931 Goni, G. J., and Trinanes, J. A. (2003). Ocean thermal structure monitoring could aid in the
932 intensity forecast of tropical cyclones. *Eos Trans. Am. Geophys. Union* 84, 573–578.
- 933 Goto, Y., Yoda, K., and Sato, K. (2017). Asymmetry hidden in birds’ tracks reveals wind,
934 heading, and orientation ability over the ocean. *Sci. Adv.* 3, e1700097.
935 doi:10.1126/sciadv.1700097.
- 936 Grodsky, S. A., Reul, N., Lagerloef, G., Reverdin, G., Carton, J. A., Chapron, B., et al. (2012).
937 Haline hurricane wake in the Amazon/Orinoco plume: AQUARIUS/SACD and SMOS
938 observations. *Geophys. Res. Lett.* 39. doi:10.1029/2012GL053335.
- 939 Haarsma, R. J., Roberts, M. J., Vidale, P. L., Senior, C. A., Bellucci, A., Bao, Q., et al. (2016).
940 High Resolution Model Intercomparison Project (HighResMIP v1.0) for CMIP6. *Geosci.*
941 *Model Dev.* 9, 4185–4208. doi:https://doi.org/10.5194/gmd-9-4185-2016.

- 942 Halliwell, G. R. H., Mehari, M. F., Hénaff, M. L., Kourafalou, V. H., Androulidakis, I. S.,
943 Kang, H. S., et al. (2017a). North Atlantic Ocean OSSE system: Evaluation of operational
944 ocean observing system components and supplemental seasonal observations for potentially
945 improving tropical cyclone prediction in coupled systems. *J. Oper. Oceanogr.* 10, 154–175.
946 doi:10.1080/1755876X.2017.1322770.
- 947 Halliwell, G. R., Mehari, M., Shay, L. K., Kourafalou, V. H., Kang, H., Kim, H.-S., et al.
948 (2017b). OSSE quantitative assessment of rapid-response prestorm ocean surveys to
949 improve coupled tropical cyclone prediction. *J. Geophys. Res. Oceans* 122, 5729–5748.
950 doi:10.1002/2017JC012760.
- 951 Halliwell, G. R., Shay, L. K., Brewster, J. K., and Teague, W. J. (2011). Evaluation and
952 sensitivity analysis of an ocean model response to Hurricane Ivan. *Mon. Weather Rev.* 139,
953 921–945. doi:10.1175/2010MWR3104.1.
- 954 Hirata, H., Kawamura, R., Kato, M., and Shinoda, T. (2015). Influential role of moisture supply
955 from the Kuroshio/Kuroshio extension in the rapid development of an extratropical cyclone.
956 *Mon. Weather Rev.* 143, 4126–4144. doi:10.1175/MWR-D-15-0016.1.
- 957 Hirata, H., Kawamura, R., Kato, M., and Shinoda, T. (2016). Response of rapidly developing
958 extratropical cyclones to sea surface temperature variations over the western Kuroshio–
959 Oyashio confluence region. *J. Geophys. Res. Atmospheres* 121, 3843–3858.
960 doi:10.1002/2015JD024391.
- 961 Hirata, H., Kawamura, R., Kato, M., and Shinoda, T. (2018). A positive feedback process
962 related to the rapid development of an extratropical cyclone over the Kuroshio/Kuroshio
963 extension. *Mon. Weather Rev.* 146, 417–433. doi:10.1175/MWR-D-17-0063.1.
- 964 Horányi, A., Cardinali, C., and Centurioni, L. (2017). The global numerical weather prediction
965 impact of mean-sea-level pressure observations from drifting buoys. *Q. J. R. Meteorol. Soc.*
966 143, 974–985. doi:10.1002/qj.2981.
- 967 Houghton, R. W., Schlitz, R., Beardsley, R. C., Butman, B., and Chamberlin, J. L. (1982). The
968 middle Atlantic Bight Cold Pool: Evolution of the temperature structure during summer
969 1979. *J. Phys. Oceanogr.* 12, 1019–1029. doi:10.1175/1520-
970 0485(1982)012<1019:TMABCP>2.0.CO;2.
- 971 Huang, B., Thorne, P. W., Banzon, V. F., Boyer, T., Chepurin, G., Lawrimore, J. H., et al.
972 (2017). Extended reconstructed sea surface temperature, Version 5 (ERSSTv5): Upgrades,
973 validations, and intercomparisons. *J. Clim.* 30, 8179–8205. doi:10.1175/JCLI-D-16-0836.1.
- 974 Huang, P., Lin, I.-I., Chou, C., and Huang, R.-H. (2015). Change in ocean subsurface
975 environment to suppress tropical cyclone intensification under global warming. *Nat.*
976 *Commun.* 6, 7188. doi:10.1038/ncomms8188.
- 977 Ingleby, B., and Isaksen, L. (2018). Drifting buoy pressures: Impact on NWP. *Atmospheric Sci.*
978 *Lett.* 19, e822. doi:10.1002/asl.822.

- 979 Jaimes, B., Shay, L. K., and Brewster, J. K. (2016). Observed air-sea interactions in tropical
980 cyclone Isaac over Loop Current mesoscale eddy features. *Dyn. Atmospheres Oceans* 76,
981 306–324. doi:10.1016/j.dynatmoce.2016.03.001.
- 982 Jayne, S. R., and Bogue, N. M. (2017). Air-Deployable profiling floats. *Oceanography* 30, 29–
983 31. Available at: <https://www.jstor.org/stable/26201841> [Accessed October 27, 2018].
- 984 Johns, E. M., Muhling, B. A., Perez, R. C., Müller-Karger, F. E., Melo, N., Smith, R. H., et al.
985 (2014). Amazon River water in the northeastern Caribbean Sea and its effect on larval reef
986 fish assemblages during April 2009. *Fish. Oceanogr.* 23, 472–494. doi:10.1111/fog.12082.
- 987 Kaneda, Y. (2010). “The advanced ocean floor real time monitoring system for megathrust
988 earthquakes and tsunamis-application of DONET and DONET2 data to seismological
989 research and disaster mitigation,” in *OCEANS 2010 MTS/IEEE*, Seattle, 1–6.
990 doi:10.1109/OCEANS.2010.5664309.
- 991 Kaplan, J., DeMaria, M., and Knaff, J. A. (2010). A revised tropical cyclone rapid
992 intensification index for the Atlantic and eastern North Pacific basins. *Weather Forecast.*
993 25, 220–241. doi:10.1175/2009WAF2222280.1.
- 994 Kelly, P. S., Lwiza, K. M. M., Cowen, R. K., and Goni, G. J. (2000). Low-salinity pools at
995 Barbados, West Indies: Their origin, frequency, and variability. *J. Geophys. Res. Oceans*
996 105, 19699–19708. doi:10.1029/1999JC900328.
- 997 Kim, H.-S., Lozano, C., Tallapragada, V., Iredell, D., Sheinin, D., Tolman, H. L., et al. (2014).
998 Performance of Ocean coupled HWRF–HYCOM model. *J. Atmospheric Ocean. Technol.*
999 31, 545–559. doi:10.1175/JTECH-D-13-00013.1.
- 1000 Knaff, J. A., Sampson, C. R., and Musgrave, K. D. (2018). An operational rapid intensification
1001 prediction aid for the western North Pacific. *Weather Forecast.* 33, 799–811.
1002 doi:10.1175/WAF-D-18-0012.1.
- 1003 Koudil, M., Charrassin, J.-B., Le Maho, Y., and Bost, C.-A. (2000). Seabirds as monitors of
1004 upper-ocean thermal structure. King penguins at the Antarctic polar front, east of Kerguelen
1005 sector. *Comptes Rendus Académie Sci. - Ser. III - Sci. Vie* 323, 377–384.
1006 doi:10.1016/S0764-4469(00)00144-X.
- 1007 Kuwano-Yoshida, A., and Asuma, Y. (2008). Numerical study of explosively developing
1008 extratropical cyclones in the northwestern Pacific region. *Mon. Weather Rev.* 136, 712–740.
1009 doi:10.1175/2007MWR2111.1.
- 1010 Kuwano-Yoshida, A., and Enomoto, T. (2013). Predictability of explosive cyclogenesis over the
1011 northwestern Pacific region using ensemble reanalysis. *Mon. Weather Rev.* 141, 3769–3785.
1012 doi:10.1175/MWR-D-12-00161.1.
- 1013 Kuwano-Yoshida, A., and Minobe, S. (2017). Storm-track response to SST fronts in the
1014 northwestern Pacific region in an AGCM. *J. Clim.* 30, 1081–1102. doi:10.1175/JCLI-D-16-
1015 0331.1.

- 1016 Kuwano-Yoshida, A., Sasaki, H., and Sasai, Y. (2017). Impact of explosive cyclones on the
1017 deep ocean in the North Pacific using an eddy-resolving ocean general circulation model.
1018 *Geophys. Res. Lett.* 44, 320–329. doi:10.1002/2016GL071367.
- 1019 Kuwano-Yoshida, A., Sasaki, H., Sasai, Y., and Hosoda, S. (2018). “Impact of explosive
1020 cyclones on the deep ocean in the North Pacific: Simulations and observations,” in
1021 *OCEANS’ 18 MTS/IEE Kobe/Techno-Ocean 2018*, Kobe, Japan.
- 1022 Landsea, C. W. (1993). A climatology of intense (or major) Atlantic hurricanes. *Mon. Weather*
1023 *Rev.* 121, 1703–1713. doi:10.1175/1520-0493(1993)121<1703:ACOIMA>2.0.CO;2.
- 1024 Lawson, R. A., Graham, D., Stalin, S., Meinig, C., Tagawa, D., Lawrence-Slavas, N., et al.
1025 (2011). “From research to commercial operations: The next generation Easy-to-Deploy
1026 (ETD) tsunami assessment buoy,” in *OCEANS 2011 IEEE*, Spain. doi:10.1109/Oceans-
1027 Spain.2011.6003520.
- 1028 Legler, D. M., Freeland, H. J., Lumpkin, R., Ball, G., McPhaden, M. J., North, S., et al. (2015).
1029 The current status of the real-time in-situ Global Ocean Observing System for operational
1030 oceanography. *J. Oper. Oceanogr.* 8, s189–s200. doi:10.1080/1755876X.2015.1049883.
- 1031 Leipper, D. F., and Volgenau, D. (1972). Hurricane heat potential of the Gulf of Mexico. *J.*
1032 *Phys. Oceanogr.* 2, 218–224. doi:10.1175/1520-0485(1972)002<0218:HHPOTG>2.0.CO;2.
- 1033 Liblik, T., Karstensen, J., Testor, P., Alenius, P., Hayes, D., Ruiz, S., et al. (2016). Potential for
1034 an underwater glider component as part of the Global Ocean Observing System. *Methods*
1035 *Oceanogr.* 17, 50–82. doi:10.1016/j.mio.2016.05.001.
- 1036 Lin, I.-I., Black, P., Price, J. F., Yang, C.-Y., Chen, S. S., Lien, C.-C., et al. (2013a). An ocean
1037 coupling potential intensity index for tropical cyclones. *Geophys. Res. Lett.* 40, 1878–1882.
1038 doi:10.1002/grl.50091.
- 1039 Lin, I.-I., Chen, C.-H., Pun, I.-F., Liu, W. T., and Wu, C.-C. (2009). Warm ocean anomaly, air
1040 sea fluxes, and the rapid intensification of tropical cyclone Nargis (2008). *Geophys. Res.*
1041 *Lett.* 36. doi:10.1029/2008GL035815.
- 1042 Lin, I.-I., Goni, G. J., Knaff, J. A., Forbes, C., and Ali, M. M. (2013b). Ocean heat content for
1043 tropical cyclone intensity forecasting and its impact on storm surge. *Nat. Hazards* 66, 1481–
1044 1500. doi:10.1007/s11069-012-0214-5.
- 1045 Lin, I.-I., Pun, I.-F., and Lien, C.-C. (2014). “Category-6” supertyphoon Haiyan in global
1046 warming hiatus: Contribution from subsurface ocean warming. *Geophys. Res. Lett.* 41,
1047 8547–8553. doi:10.1002/2014GL061281.
- 1048 Lin, I.-I., Wu, C.-C., Emanuel, K. A., Lee, I.-H., Wu, C.-R., and Pun, I.-F. (2005). The
1049 interaction of supertyphoon Maemi (2003) with a warm ocean eddy. *Mon. Weather Rev.*
1050 133, 2635–2649. doi:10.1175/MWR3005.1.
- 1051 Lin, I.-I., Wu, C.-C., Pun, I.-F., and Ko, D.-S. (2008). Upper-ocean thermal structure and the
1052 western North Pacific category 5 typhoons. Part I: Ocean features and the category 5

- 1053 typhoons' Intensification. *Mon. Weather Rev.* 136, 3288–3306.
1054 doi:10.1175/2008MWR2277.1.
- 1055 Mainelli, M., DeMaria, M., Shay, L. K., and Goni, G. (2008). Application of oceanic heat
1056 content estimation to operational forecasting of recent Atlantic category 5 hurricanes.
1057 *Weather Forecast.* 23, 3–16. doi:10.1175/2007WAF2006111.1.
- 1058 Mao, Q., Chang, S. W., and Pfeffer, R. L. (2000). Influence of large-scale initial oceanic mixed
1059 layer depth on tropical cyclones. *Mon. Weather Rev.* 128, 4058–4070. doi:10.1175/1520-
1060 0493(2000)129<4058:IOLSIO>2.0.CO;2.
- 1061 Masumoto, Y., Hermes, Beal, Roxy, Vialard, J., Andres, et al. (this issue). Sustained Indian
1062 Ocean Observing System. *Front. Mar. Sci.*
- 1063 Menkes, C. E., Lengaigne, M., Lévy, M., Ethé, C., Bopp, L., Aumont, O., et al. (2016). Global
1064 impact of tropical cyclones on primary production. *Glob. Biogeochem. Cycles* 30, 767–786.
1065 doi:10.1002/2015GB005214.
- 1066 Meyers, P. C., Shay, L. K., and Brewster, J. K. (2014). Development and analysis of the
1067 systematically merged Atlantic regional temperature and salinity climatology for oceanic
1068 heat content estimates. *J. Atmospheric Ocean. Technol.* 31, 131–149. doi:10.1175/JTECH-
1069 D-13-00100.1.
- 1070 Meyers, P. C., Shay, L. K., Brewster, J. K., and Jaimes, B. (2015). Observed ocean thermal
1071 response to Hurricanes Gustav and Ike. *J. Geophys. Res. Oceans* 121, 162–179.
1072 doi:10.1002/2015JC010912.
- 1073 Miles, T., Seroka, G., and Glenn, S. (2017). Coastal ocean circulation during Hurricane Sandy.
1074 *J. Geophys. Res. Oceans* 122, 7095–7114. doi:10.1002/2017JC013031.
- 1075 Miles, T., Seroka, G., Kohut, J., Schofield, O., and Glenn, S. (2015). Glider observations and
1076 modeling of sediment transport in Hurricane Sandy. *J. Geophys. Res. Oceans* 120, 1771–
1077 1791. doi:10.1002/2014JC010474.
- 1078 Miyazawa, Y., Guo, X., Varlamov, S. M., Miyama, T., Yoda, K., Sato, K., et al. (2015).
1079 Assimilation of the seabird and ship drift data in the north-eastern sea of Japan into an
1080 operational ocean nowcast/forecast system. *Sci. Rep.* 5, 17672. doi:10.1038/srep17672.
- 1081 Mochizuki, M., Kanazawa, T., Uehira, K., Shimbo, T., Shiomi, K., Kunugi, T., et al. (2017). “S-
1082 net project: Construction of large scale seafloor observatory network for tsunamis and
1083 earthquakes in Japan,” in *AGU Fall Meeting 2017*, New Orleans, Louisiana.
- 1084 Narazaki, T., Sato, K., Abernathy, K. J., Marshall, G. J., and Miyazaki, N. (2009). Sea turtles
1085 compensate deflection of heading at the sea surface during directional travel. *J. Exp. Biol.*
1086 212, 4019–4026. doi:10.1242/jeb.034637.
- 1087 Neetu, S., Lengaigne, M., Vincent, E. M., Vialard, J., Madec, G., Samson, G., et al. (2012).
1088 Influence of upper-ocean stratification on tropical cyclone-induced surface cooling in the
1089 Bay of Bengal. *J. Geophys. Res. Oceans* 117. doi:10.1029/2012JC008433.

- 1090 Nishida, K., and Takagi, R. (2016). Teleseismic S wave microseisms. *Science* 353, 919–921.
1091 doi:10.1126/science.aaf7573.
- 1092 Perry, R. L., Leung, P. T., Bouchard, R., Petraitis, D., Smith, W. C., Sharma, N., et al. (2017).
1093 “The continuation of an ocean observing collaboration to improve hurricane and loop
1094 current forecasting and modeling in the Gulf of Mexico,” in *OCEANS 2017*, Anchorage, 1–
1095 7.
- 1096 Pickard, G. L., and Emery, W. J. (1990). *Descriptive Physical Oceanography*. Pergamon, New
1097 York.
- 1098 Price, J. F. (2009). Metrics of hurricane-ocean interaction: vertically-integrated or vertically-
1099 averaged ocean temperature? *Ocean Sci* 5, 351–368. doi:10.5194/os-5-351-2009.
- 1100 Riser, S. C., Freeland, H. J., Roemmich, D., Wijffels, S., Troisi, A., Belbéoch, M., et al. (2016).
1101 Fifteen years of ocean observations with the global Argo array. *Nat. Clim. Change* 6, 145–
1102 153. doi:10.1038/nclimate2872.
- 1103 Rogers, R. F., Aberson, S., Bell, M. M., Cecil, D. J., Doyle, J. D., Kimberlain, T. B., et al.
1104 (2017). Rewriting the tropical record books: The extraordinary intensification of Hurricane
1105 Patricia (2015). *Bull. Am. Meteorol. Soc.* 98, 2091–2112. doi:10.1175/BAMS-D-16-0039.1.
- 1106 Rudnick, D. L. (2016). Ocean Research Enabled by Underwater Gliders. *Annu. Rev. Mar. Sci.* 8,
1107 519–541. doi:10.1146/annurev-marine-122414-033913.
- 1108 Rudzin, J. E., Shay, L. K., Jaimes, B., and Brewster, J. K. (2017). Upper ocean observations in
1109 eastern Caribbean Sea reveal barrier layer within a warm core eddy. *J. Geophys. Res.*
1110 *Oceans* 122, 1057–1071. doi:10.1002/2016JC012339.
- 1111 Rudzin, J. E., Shay, L. K., and Johns, W. E. (2018). The influence of the barrier layer on SST
1112 response during tropical cyclone wind forcing using idealized experiments. *J. Phys.*
1113 *Oceanogr.* 48, 1471–1478. doi:10.1175/JPO-D-17-0279.1.
- 1114 Sanabia, E. R., Barrett, B. S., Black, P. G., Chen, S., and Cummings, J. A. (2013). Real-time
1115 upper-ocean temperature observations from aircraft during operational hurricane
1116 reconnaissance missions: AXBT demonstration project year one results. *Weather Forecast.*
1117 28, 1404–1422. doi:10.1175/WAF-D-12-00107.1.
- 1118 Sanders, F., and Gyakum, J. R. (1980). Synoptic-Dynamic climatology of the “Bomb.” *Mon.*
1119 *Weather Rev.* 108, 1589–1606. doi:10.1175/1520-0493(1980)108<1589:SDCOT>2.0.CO;2.
- 1120 Sanford, T. B., Black, P. G., Haustein, J. R., Feeney, J. W., Forristall, G. Z., and Price, J. F.
1121 (1987). Ocean response to a hurricane. Part I: Observations. *J. Phys. Oceanogr.* 17, 2065–
1122 2083. doi:10.1175/1520-0485(1987)017<2065:ORTAHP>2.0.CO;2.
- 1123 Sanford, T. B., Price, J. F., and Girton, J. B. (2011). Upper-ocean response to Hurricane Frances
1124 (2004) observed by profiling EM-APEX floats. *J. Phys. Oceanogr.* 41, 1041–1056.
1125 doi:10.1175/2010JPO4313.1.

- 1126 Sanford, T. B., Price, J. F., Girton, J. B., and Webb, D. C. (2007). Highly resolved observations
 1127 and simulations of the ocean response to a hurricane. *Geophys. Res. Lett.* 34.
 1128 doi:10.1029/2007GL029679.
- 1129 Seroka, G., Miles, T., Xu, Y., Kohut, J., Schofield, O., and Glenn, S. (2016). Hurricane Irene
 1130 sensitivity to stratified coastal ocean cooling. *Mon. Weather Rev.* 144, 3507–3530.
 1131 doi:10.1175/MWR-D-15-0452.1.
- 1132 Shapiro, M., Wernli, H., Bao, J.-W., Methven, J., Zou, X., Doyle, J., et al. (1999). “A Planetary-
 1133 Scale to Mesoscale Perspective of the Life Cycles of Extratropical Cyclones: The Bridge
 1134 between Theory and Observations,” in *The Life Cycles of Extratropical Cyclones*, eds. M.
 1135 A. Shapiro and S. Grønås (Boston, MA: American Meteorological Society), 139–185.
 1136 doi:10.1007/978-1-935704-09-6_14.
- 1137 Shay, L. K., Ali, M. M., Chen, S., Ginis, I., Halliwell, G., Kim, H., et al. (2014). “Air-sea
 1138 Interface and Oceanic Influences (Topic 4.4)”, Jeju, Republic of Korea: World
 1139 Meteorological Organization (WMO).
- 1140 Shay, L. K., Black, P. G., Mariano, A. J., Hawkins, J. D., and Elsberry, R. L. (1992). Upper
 1141 ocean response to Hurricane Gilbert. *J. Geophys. Res. Oceans* 97, 20227–20248.
 1142 doi:10.1029/92JC01586.
- 1143 Shay, L. K., and Brewster, J. K. (2010). Oceanic heat content variability in the eastern Pacific
 1144 Ocean for hurricane intensity forecasting. *Mon. Weather Rev.* 138, 2110–2131.
 1145 doi:10.1175/2010MWR3189.1.
- 1146 Shay, L. K., Goni, G. J., and Black, P. G. (2000). Effects of a warm oceanic feature on
 1147 Hurricane Opal. *Mon. Weather Rev.* 128, 1366–1383. doi:10.1175/1520-
 1148 0493(2000)128<1366:EOAWOF>2.0.CO;2.
- 1149 Smith, E. R., Kessel, W., Cravatte, S., Sprintall, S., Cronin, S., Sutton, M., et al. (this issue).
 1150 Tropical Pacific Observing System. *Front. Mar. Sci.*
- 1151 Sprintall, J., and Tomczak, M. (1992). Evidence of the barrier layer in the surface layer of the
 1152 tropics. *J. Geophys. Res. Oceans* 97, 7305–7316. doi:10.1029/92JC00407.
- 1153 Testor, P., Rudnick, D. L., Pattiaratchi, C., Pallas, E., and Rehm, E. (this issue). Ocean Gliders:
 1154 a component of the integrated GOOS. *Front. Mar. Sci.*
- 1155 Todd, R. E., Chavez, F., Clayton, S., Cravatte, S., Pereira, M., Graco, M., et al. (this issue).
 1156 Global perspectives on observing ocean boundary current systems. *Front. Mar. Sci.*
- 1157 Todd, R. E., Asher, T. G., Heiderich, J., Bane, J. M., and Luettich, R. A. (2018). Transient
 1158 response of the Gulf Stream to multiple hurricanes in 2017. *Geophys. Res. Lett.* 45, 10,509-
 1159 10,519. doi:10.1029/2018GL079180.
- 1160 Todd, R. E., Rudnick, D. L., Sherman, J. T., Owens, W. B., and George, L. (2017). Absolute
 1161 velocity estimates from autonomous underwater gliders equipped with Doppler current
 1162 profilers. *J. Atmospheric Ocean. Technol.* 34, 309–333. doi:10.1175/JTECH-D-16-0156.1.

- 1163 Trenberth, K. E., Cheng, L., Jacobs, P., Zhang, Y., and Fasullo, J. (2018). Hurricane Harvey
 1164 Links to Ocean Heat Content and Climate Change Adaptation. *Earths Future* 6, 730–744.
 1165 doi:10.1029/2018EF000825.
- 1166 Ulbrich, U., Leckebusch, G. C., and Pinto, J. G. (2009). Extra-tropical cyclones in the present
 1167 and future climate: a review. *Theor. Appl. Climatol.* 96, 117–131. doi:10.1007/s00704-008-
 1168 0083-8.
- 1169 Venugopal, T., Ali, M. M., Bourassa, M. A., Zheng, Y., Goni, G. J., Foltz, G. R., et al. (2018).
 1170 Statistical evidence for the role of southwestern Indian Ocean heat content in the Indian
 1171 summer monsoon rainfall. *Sci. Rep.* 8, 12092. doi:10.1038/s41598-018-30552-0.
- 1172 Wada, A., Kunii, M., Yonehara, Y., and Sato, K. (2017). “Impacts on local heavy rainfalls of
 1173 surface winds measurement by seabirds,” in *CAS/JSC WGNE Res. Activities in Atm. And.*
 1174 *Oceanic Modelling*, 25.
- 1175 Wang, X., Han, G., Qi, Y., and Li, W. (2011). Impact of barrier layer on typhoon-induced sea
 1176 surface cooling. *Dyn. Atmospheres Oceans* 52, 367–385.
 1177 doi:10.1016/j.dynatmoce.2011.05.002.
- 1178 Watanuki, Y., Mehlum, F., and Takahashi, A. (2001). Water temperature sampling by foraging
 1179 Brünnich’s Guillemots with bird-borne data loggers. *J. Avian Biol.* 32, 189–193.
 1180 doi:10.1034/j.1600-048X.2001.320214.x.
- 1181 Wilson, R. P., Grémillet, D., Syder, J., Kierspel, M. A. M., Garthe, S., Weimerskirch, H., et al.
 1182 (2002). Remote-sensing systems and seabirds: their use, abuse and potential for measuring
 1183 marine environmental variables. *Mar. Ecol. Prog. Ser.* 228, 241–261.
 1184 doi:10.3354/meps228241.
- 1185 World Meteorological Organization (WMO) (2015a). Manual on Codes (WMO 306). Geneva:
 1186 World Meteorological Organization.
- 1187 World Meteorological Organization (WMO) (2015b). Manual on the Global
 1188 Telecommunication System (WMO 386). Geneva: World Meteorological Organization.
- 1189 Wu, L., Cai, W., Zhang, L., Nakamura, H., Timmermann, A., Joyce, T., et al. (2012). Enhanced
 1190 warming over the global subtropical western boundary currents. *Nat. Clim. Change* 2, 161–
 1191 166. doi:10.1038/nclimate1353.
- 1192 Yamaguchi, M., Owada, H., Shimada, U., Sawada, M., Iriguchi, T., Musgrave, K. D., et al.
 1193 (2018). Tropical cyclone intensity prediction in the western North Pacific basin using
 1194 SHIPS and JMA/GSM. *SOLA* 14, 138–143. doi:10.2151/sola.2018-024.
- 1195 Yoda, K., Shiomi, K., and Sato, K. (2014). Foraging spots of streaked shearwaters in relation to
 1196 ocean surface currents as identified using their drift movements. *Prog. Oceanogr.* 122, 54–
 1197 64. doi:10.1016/j.pocean.2013.12.002.
- 1198 Yonehara, Y., Goto, Y., Yoda, K., Watanuki, Y., Young, L. C., Weimerskirch, H., et al. (2016).
 1199 Flight paths of seabirds soaring over the ocean surface enable measurement of fine-scale

- 1200 wind speed and direction. *Proc. Natl. Acad. Sci.* 113, 9039–9044.
1201 doi:10.1073/pnas.1523853113.
- 1202 Yoshida, A., and Asuma, Y. (2004). Structures and environment of explosively developing
1203 extratropical cyclones in the northwestern Pacific region. *Mon. Weather Rev.* 132, 1121–
1204 1142. doi:10.1175/1520-0493(2004)132<1121:SAEOED>2.0.CO;2.
- 1205 Zhang, H.-M., Reynolds, R. W., Lumpkin, R., Molinari, R., Arzayus, K., Johnson, M., et al.
1206 (2009). An integrated global observing system for sea surface temperature using satellites
1207 and in-situ data: Research to operations. *Bull. Am. Meteorol. Soc.* 90, 31–38.
1208 doi:10.1175/2008BAMS2577.1.
- 1209 Zhang, J. A., Atlas, R., Emmitt, G. D., Bucci, L., and Ryan, K. (2018). Airborne Doppler wind
1210 lidar observations of the tropical cyclone boundary layer. *Remote Sens.* 10, 825.
1211 doi:10.3390/rs10060825.
- 1212 Zhang, J. A., Black, P. G., French, J. R., and Drennan, W. M. (2008). First direct measurements
1213 of enthalpy flux in the hurricane boundary layer: The CBLAST results. *Geophys. Res. Lett.*
1214 35. doi:10.1029/2008GL034374.
- 1215 Zhang, J. A., Nolan, D. S., Rogers, R. F., and Tallapragada, V. (2015). Evaluating the impact of
1216 improvements in the boundary layer parameterization on hurricane intensity and structure
1217 forecasts in HWRF. *Mon. Weather Rev.* 143, 3136–3155. doi:10.1175/MWR-D-14-00339.1.
- 1218 Zhou, L., Chen, D., Karnauskas, K. B., Wang, C., Lei, X., Wang, W., et al. (2018). Introduction
1219 to special section on oceanic responses and feedbacks to tropical cyclones. *J. Geophys. Res.*
1220 *Oceans* 123, 742–745. doi:10.1002/2018JC013809.
- 1221

Figure Captions

1222
1223
1224
1225
1226
1227
1228
1229
1230
1231
1232
1233
1234
1235
1236
1237
1238
1239
1240
1241
1242
1243
1244
1245
1246
1247
1248
1249
1250
1251
1252
1253
1254
1255
1256
1257
1258
1259

Figure 1. Global TC tracks during the time period of 1993-2011, overlaid on the average hurricane season satellite-derived Tropical Cyclone Heat Potential (upper ocean heat content above 26 °C isotherm) for each hemisphere computed for the same period. Thin white lines show the tracks of TCs with Cat-2 and below, and red lines show tracks of major TCs with Cat-3 and above.

Figure 2. Track of Hurricane Katrina (2005) overlaid on tropical cyclone heat potential (TCHP, upper ocean heat content) conditions in the Gulf of Mexico on 08/20/2005 (prior to the passage of Katrina). Gray contours are displayed every 5 kJ cm⁻² units.

Figure 3. Official Atlantic hurricane intensity forecast error for the Atlantic basin reported by NOAA's National Hurricane Center⁸.

Figure 4. (a) Satellite tracks of 15 loggerhead turtles released from Sanriku coast, Japan (open circle) between 2010 and 2014. (b) Tracks of 33 Streaked shearwaters from a breeding colony in Funakoshi-Ohshima Island, Japan (open circle) between August and September in 2013 and 2014.

Figure 5. Scatter between 36-hour intensity changes of Atlantic TCs and SST (red), TCHP (blue), and Tdy (magenta) for the 10-yr period 2005–14. (a)–(c) All storm locations, (d)–(f) cases where the magnitude of the hurricane-induced SST cooling is below 0.5 °C, and (g)–(i) cases where the cold wake magnitude is greater than 0.5 °C. Correlation coefficients are also indicated in each panel. Reproduced from Balaguru et al., (2018).

Figure 6. (a) Tracks of Hurricanes Gonzalo (2014) and Fay (2014) superimposed on the altimetry-derived upper ocean heat content (tropical cyclone heat potential) during October 2014. (b) Impact of glider temperature profiles on the initialization of HYCOM-HWRF. (c) Impact of glider and other ocean data to reduce errors in TC intensity (maximum wind speed) during the forecast of Gonzalo tested on October 13, 2014. Figure adapted from Goni et al. (2017).

Figure 7. North Atlantic sea surface temperature forecasts: (a) observed and (b) forecast mean Atlantic SST anomalies during September 2017. Solid and dotted black line shows location of the 26.5 °C isotherm during September 2017 relative to September 1993–2015. (c) Observed and (d) forecast mean Atlantic SSTs during September 2017. Anomalies relative to September 1993–2015. Adapted from Camp et al., (2018).

⁸ source: <https://www.nhc.noaa.gov/verification/verify5.shtml>

1260 **Figure 8.** (a) Barrier layer thickness (BLT) calculated using underwater glider observations
1261 collected in areas off Puerto Rico under major 2017 TCs. (b) Average surface chlorophyll
1262 concentration for August 2017 derived from MODIS-Aqua data. Major rivers contributing to
1263 elevated chlorophyll concentrations are indicated. (c) Chlorophyll anomalies during hurricane
1264 season in the Tropical North Atlantic (TNA) Ocean for areas off Puerto Rico. (d) Same as (c),
1265 but for areas in the Caribbean Sea (CAR) off Puerto Rico.

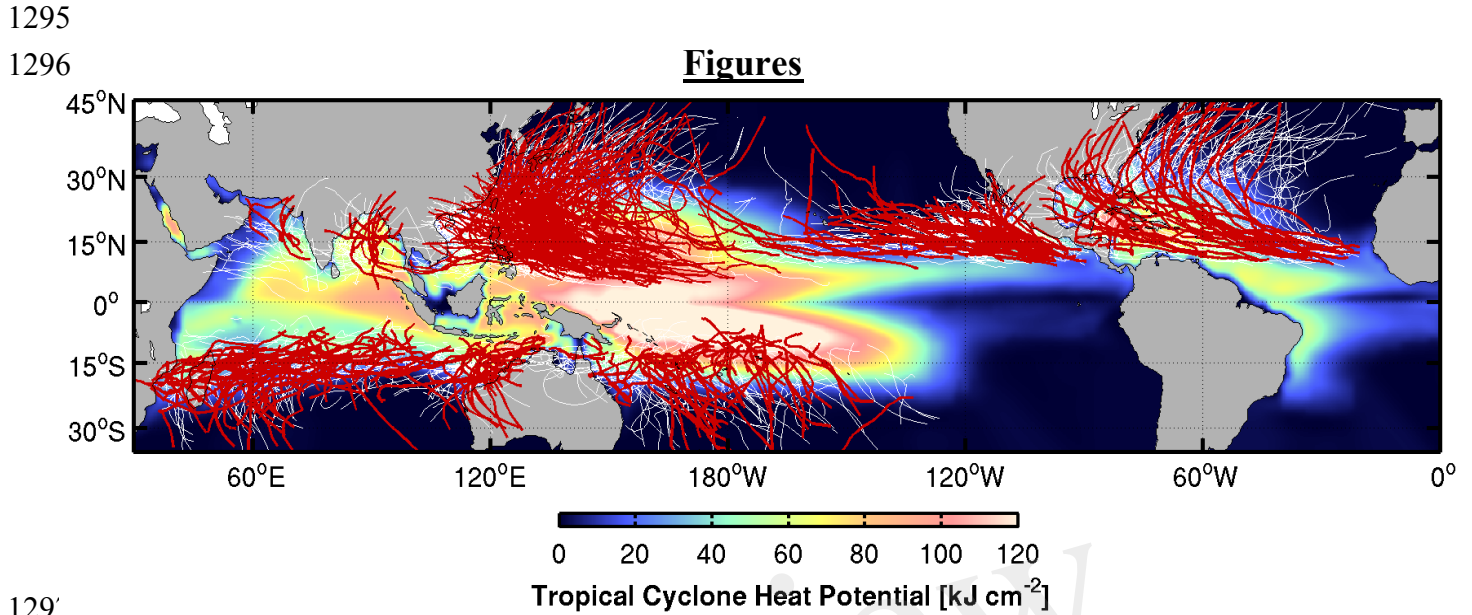
1266
1267 **Figure 9.** The separation of a LC WCE during the passage of Hurricane Nate of 2017. The color
1268 scale is for ocean heat content (OHC) relative to the 26 °C isotherm, from the satellite fields
1269 (Meyers et al., 2014). APEX-EM floats (purple, white, red, and yellow dots) that were active
1270 during Nate's passage of Nate over the Gulf. (a) Pre-storm OHC structure on 5 October 2017. (b)
1271 Post-storm OHC structure on 10 October 2017. Black dots in (a) and (b) depict airborne ocean
1272 profilers deployed from NOAA WP-3D research aircraft; green, blue, and red stars in (b)
1273 represent in-storm oceanographic and atmospheric airborne profilers.

1274
1275 **Figure 10.** Background color map of average temperature for the upper 100 m (T100) from the
1276 East Asia Seas Nowcast/Forecast System on 23 September 2010. Overlaid are graphical
1277 representations of the ITOP operations area, experimental tools, and strategy. Locations of the
1278 three major ITOP storms at the time of maximum sampling are shown by storm symbols. Figure
1279 originally from D'Asaro et al. (2014), ©American Meteorological Society. Used with
1280 permission.

1281
1282 **Figure 11.** Evolution of temperature and air–sea fluxes for three ITOP TCs (Megi, Fanapi, and
1283 Malakas). (a) Pre-TC temperature profiles from ARGO floats. (b) Symbols: SST and air
1284 temperature at the core of each TC as measured by dropsonde/AXBT pairs. Lines: results of an
1285 ocean model (Price et al., 1994) driven by the observed TC (solid) and extrapolated to higher
1286 wind speeds (dashed). (c) As in (b), but for estimated total enthalpy flux (After Lin et al. GRL,
1287 2013).

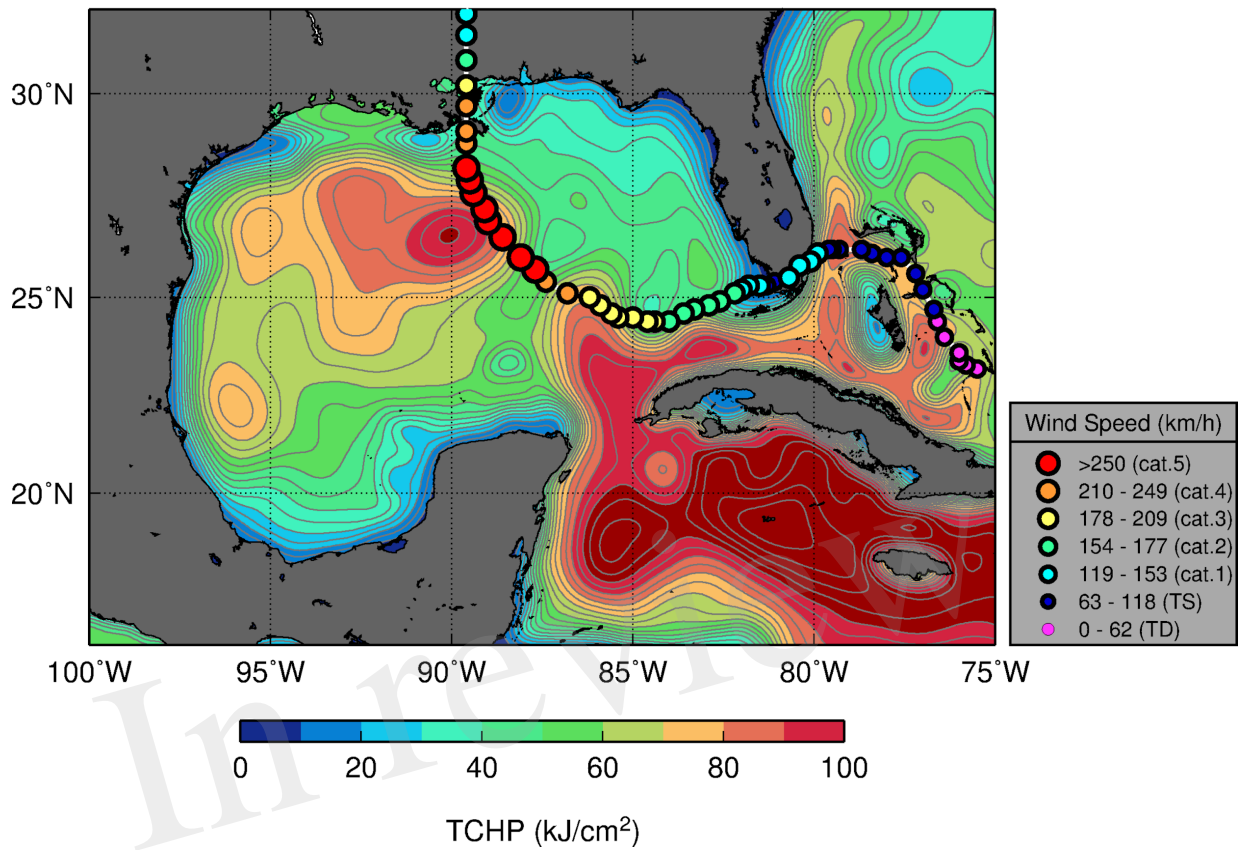
1288
1289 **Figure 12.** Mean fields of TCHP (a, c, and e) and H_{26} (b, d, and f) averaged over the time
1290 interval 21 August through 8 October 2017. Observation-based estimates are provided by the
1291 NOAA/AOML TCHP product (a and b). Model fields are from an unconstrained simulation (c
1292 and d) and from an analysis that assimilated all ocean profilers (Argo floats, underwater gliders,
1293 and Alamo floats).

1294



1297
1298 **Figure 1.** Global TC tracks during the time period of 1993-2011, overlaid on the average
1299 hurricane season satellite-derived Tropical Cyclone Heat Potential (upper ocean heat content
1300 above 26 °C isotherm) for each hemisphere computed for the same period. Thin white lines show
1301 the tracks of TCs with Cat-2 and below, and red lines show tracks of major TCs with Cat-3 and
1302 above.
1303

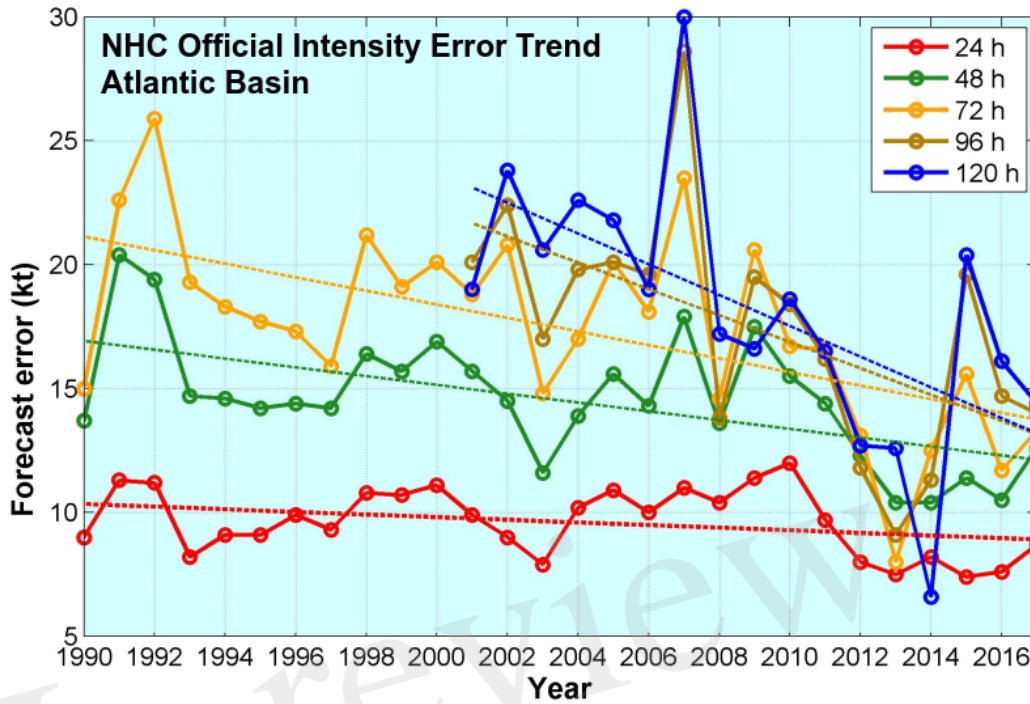
1304



1305
1306
1307
1308
1309

Figure 2. Track of Hurricane Katrina (2005) overlaid on tropical cyclone heat potential (TCHP, upper ocean heat content) conditions in the Gulf of Mexico on 08/20/2005 (prior to the passage of Katrina). Gray contours are displayed every 5 kJ cm⁻² units.

1310

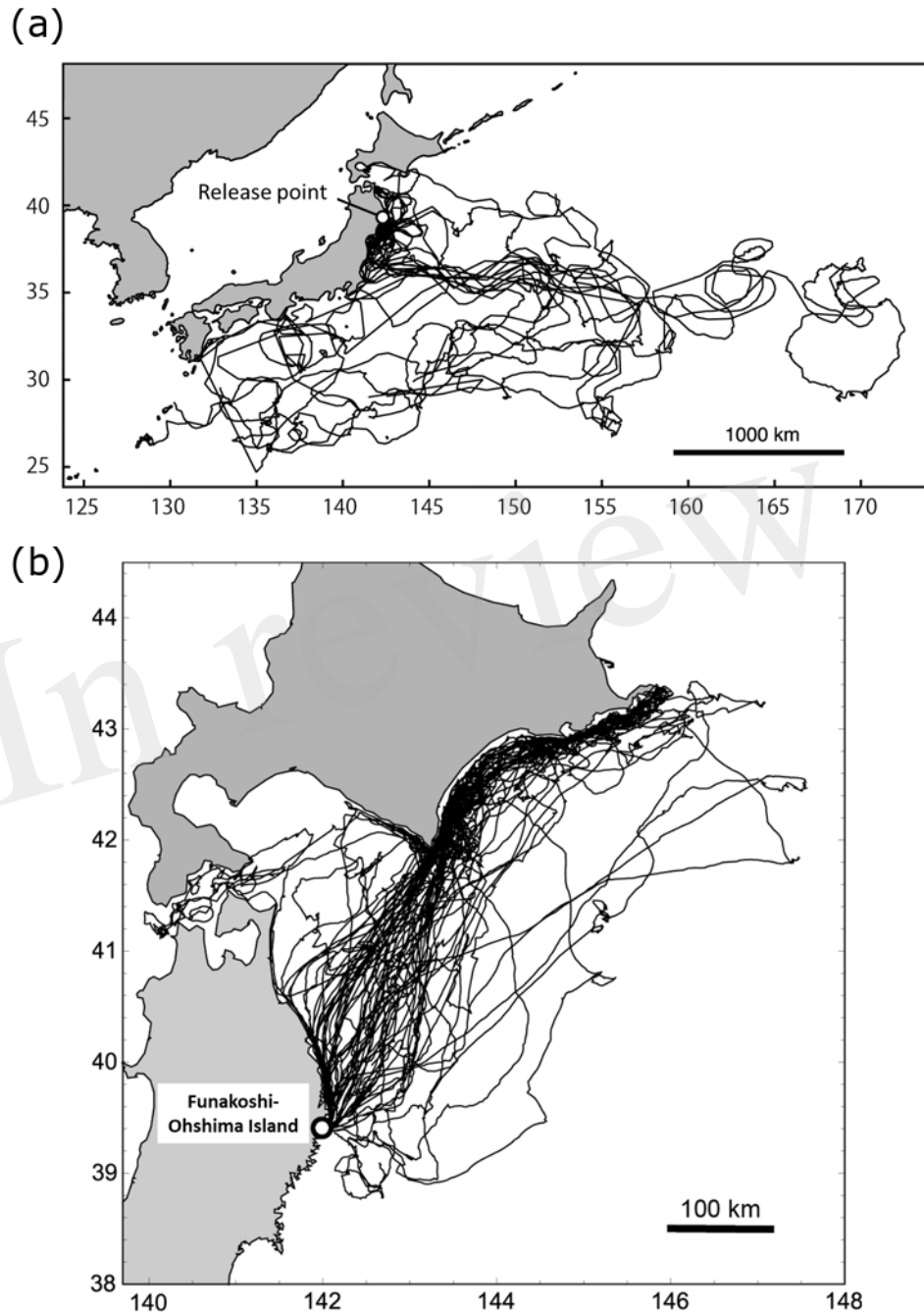


1311
1312
1313
1314

Figure 3. Official Atlantic hurricane intensity forecast error for the Atlantic basin reported by NOAA’s National Hurricane Center⁹.

⁹ source: <https://www.nhc.noaa.gov/verification/verify5.shtml>

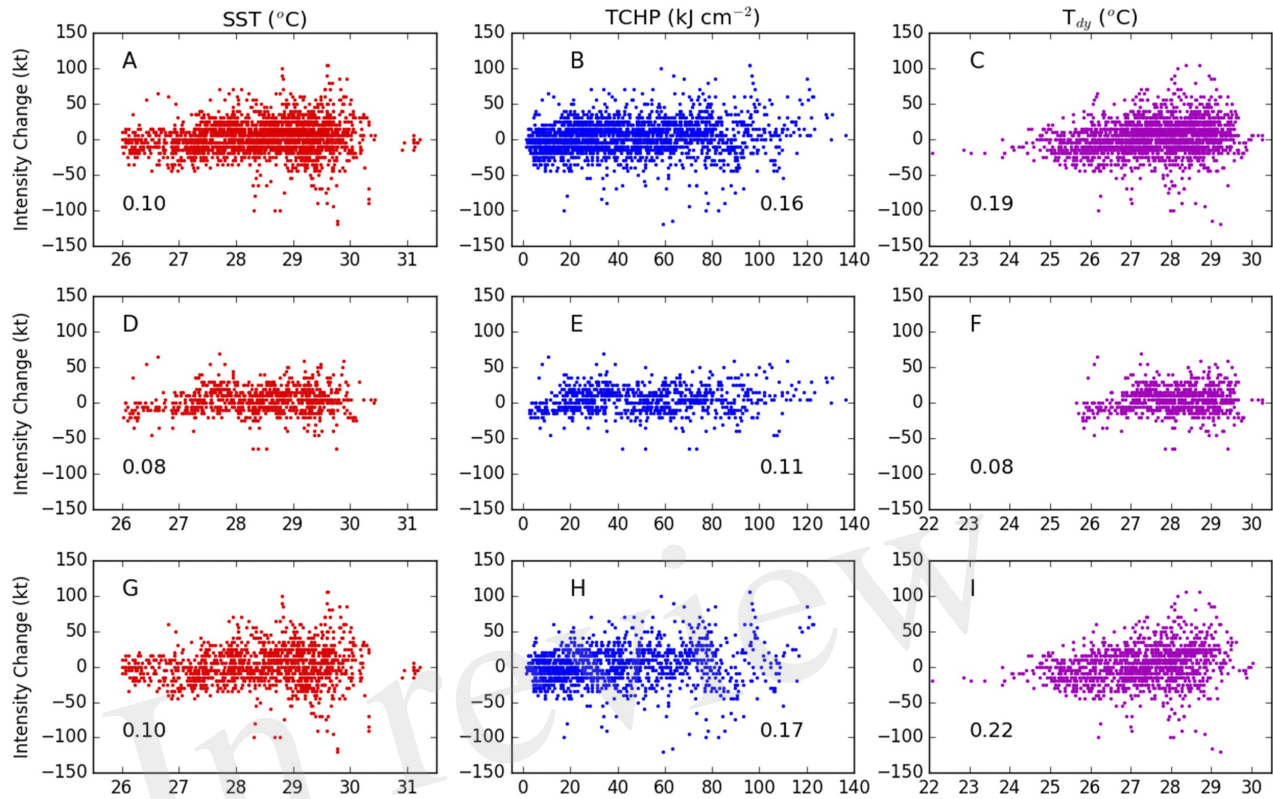
1315



1316
1317
1318
1319
1320
1321

Figure 4. (a) Satellite tracks of 15 loggerhead turtles released from Sanriku coast, Japan (open circle) between 2010 and 2014. (b) Tracks of 33 Streaked shearwaters from a breeding colony in Funakoshi-Oshima Island, Japan (open circle) between August and September in 2013 and 2014.

1322



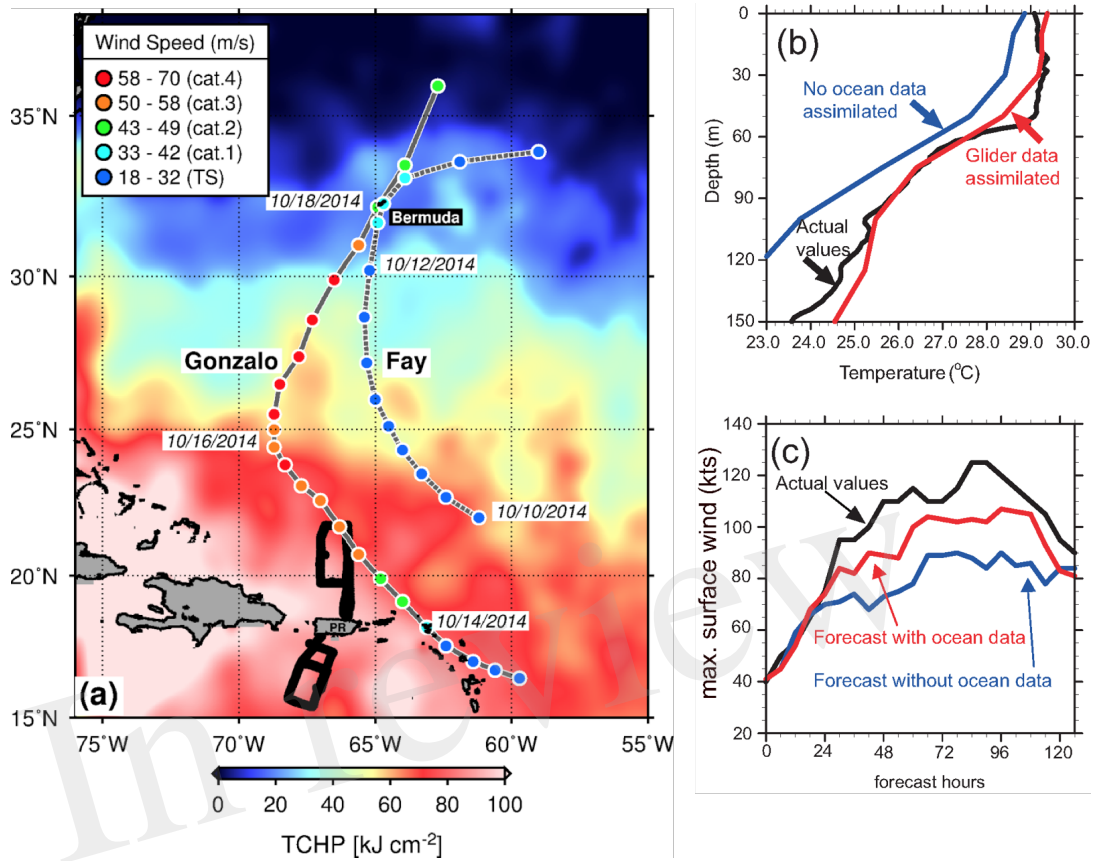
1323

1324

1325 **Figure 5.** Scatter between 36-hour intensity changes of Atlantic TCs and SST (red), TCHP
 1326 (blue), and Tdy (magenta) for the 10-yr period 2005–14. (a)–(c) All storm locations, (d)–(f)
 1327 cases where the magnitude of the hurricane-induced SST cooling is below 0.5 °C, and (g)–(i)
 1328 cases where the cold wake magnitude is greater than 0.5 °C. Correlation coefficients are also
 1329 indicated in each panel. Reproduced from Balaguru et al., (2018)

1330

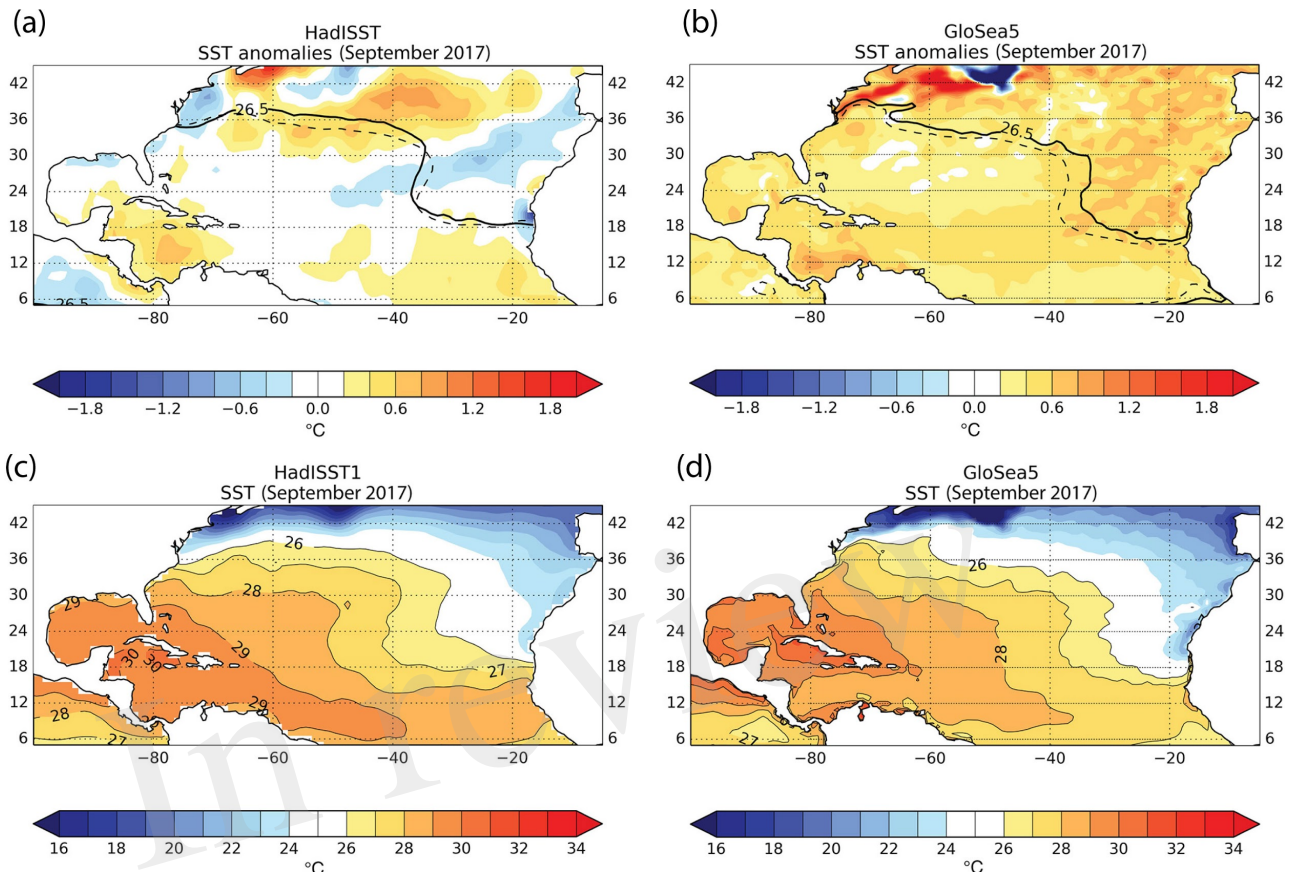
1331



1332
 1333
 1334
 1335
 1336
 1337
 1338
 1339

Figure 6. (a) Tracks of Hurricanes Gonzalo (2014) and Fay (2014) superimposed on the altimetry-derived upper ocean heat content (tropical cyclone heat potential) during October 2014. (b) Impact of glider temperature profiles on the initialization of HYCOM-HWRF. (c) Impact of glider and other ocean data to reduce errors in TC intensity (maximum wind speed) during the forecast of Gonzalo tested on October 13, 2014. Figure adapted from Goni et al. (2017).

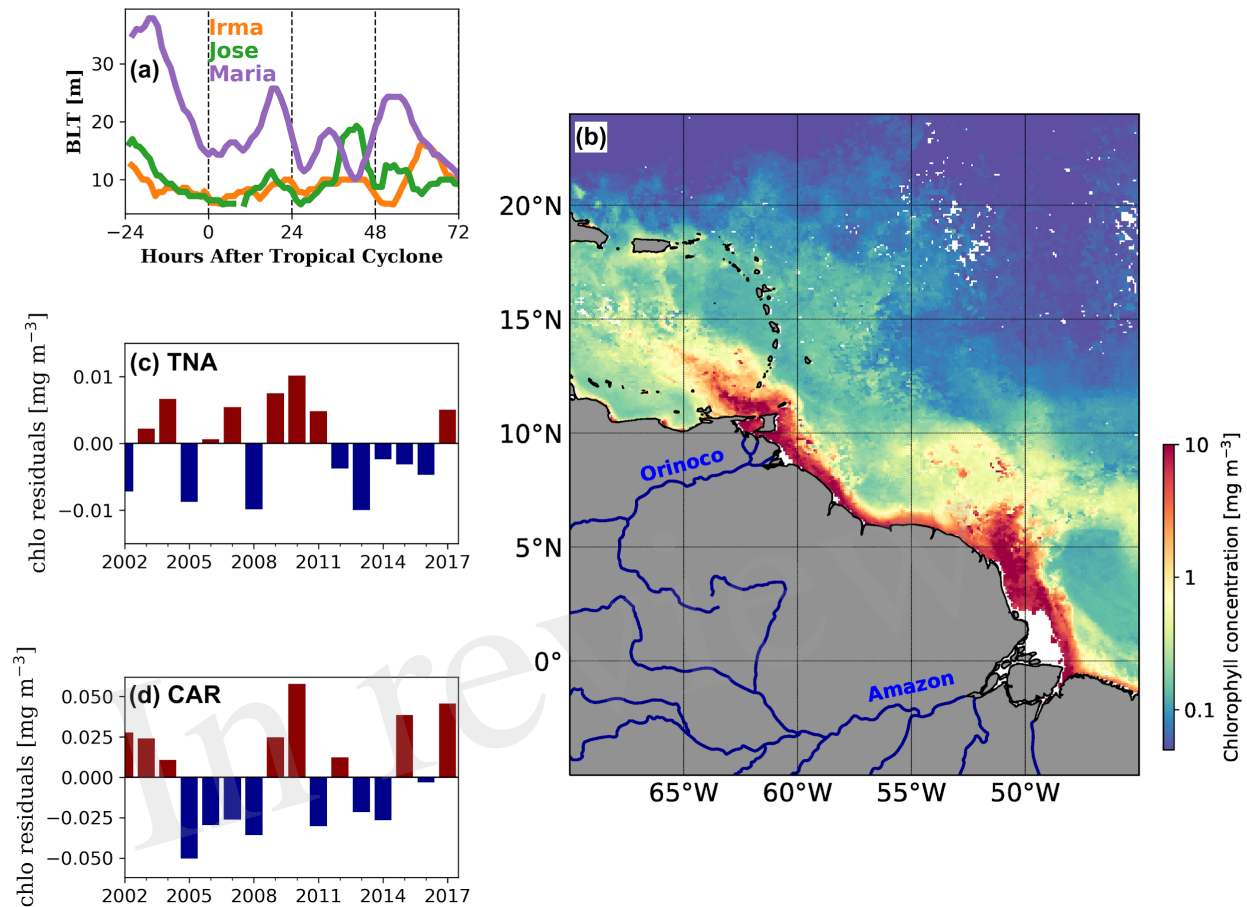
1340



1341
1342
1343
1344
1345
1346
1347
1348
1349

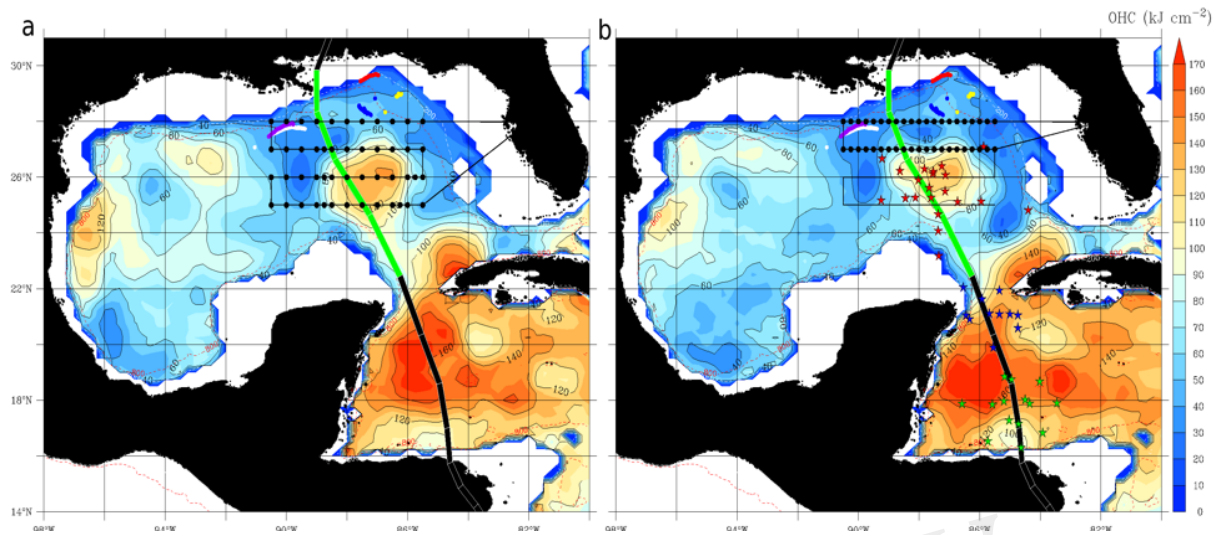
Figure 7. North Atlantic sea surface temperature forecasts: (a) observed and (b) forecast mean Atlantic SST anomalies during September 2017. Solid and dotted black line shows location of the 26.5 °C isotherm during September 2017 relative to September 1993–2015. (c) Observed and (d) forecast mean Atlantic SSTs during September 2017. Anomalies relative to September 1993–2015. Adapted from Camp et al., (2018).

1350

1351
1352

1353 **Figure 8.** (a) Barrier layer thickness (BLT) calculated using underwater glider observations
 1354 collected in areas off Puerto Rico under major 2017 TCs. (b) Average surface chlorophyll
 1355 concentration for August 2017 derived from MODIS-Aqua data. Major rivers contributing to
 1356 elevated chlorophyll concentrations are indicated. (c) Chlorophyll anomalies during hurricane
 1357 season in the Tropical North Atlantic (TNA) Ocean for areas off Puerto Rico. (d) Same as (c),
 1358 but for areas in the Caribbean Sea (CAR) off Puerto Rico.
 1359

1360



1361

1362

1363

1364

1365

1366

1367

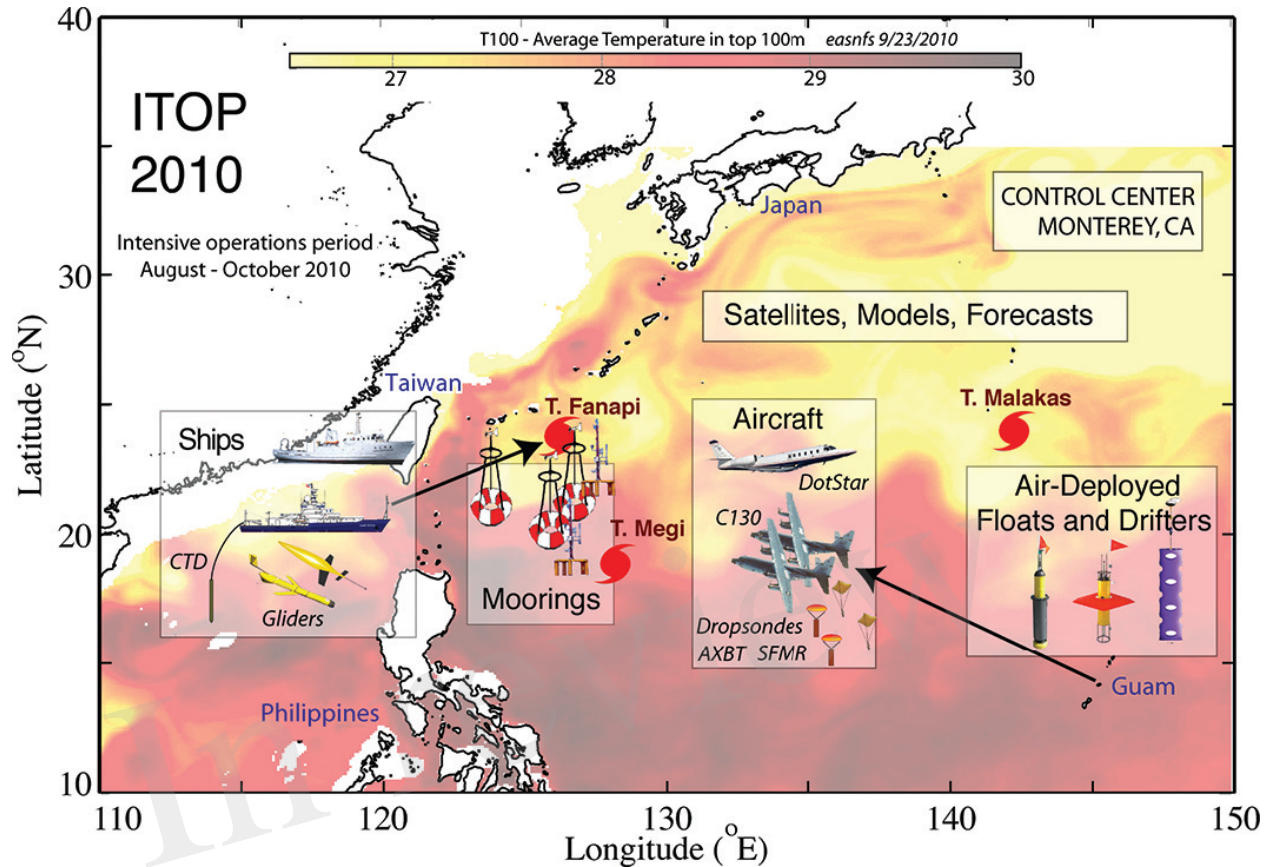
1368

1369

1370

Figure 9. The separation of a LC WCE during the passage of Hurricane Nate of 2017. The color scale is for ocean heat content (OHC) relative to the 26 °C isotherm, from the satellite fields (Meyers et al., 2014). APEX-EM floats (purple, white, red, and yellow dots) that were active during Nate's passage of Nate over the Gulf. (a) Pre-storm OHC structure on 5 October 2017. (b) Post-storm OHC structure on 10 October 2017. Black dots in (a) and (b) depict airborne ocean profilers deployed from NOAA WP-3D research aircraft; green, blue, and red stars in (b) represent in-storm oceanographic and atmospheric airborne profilers.

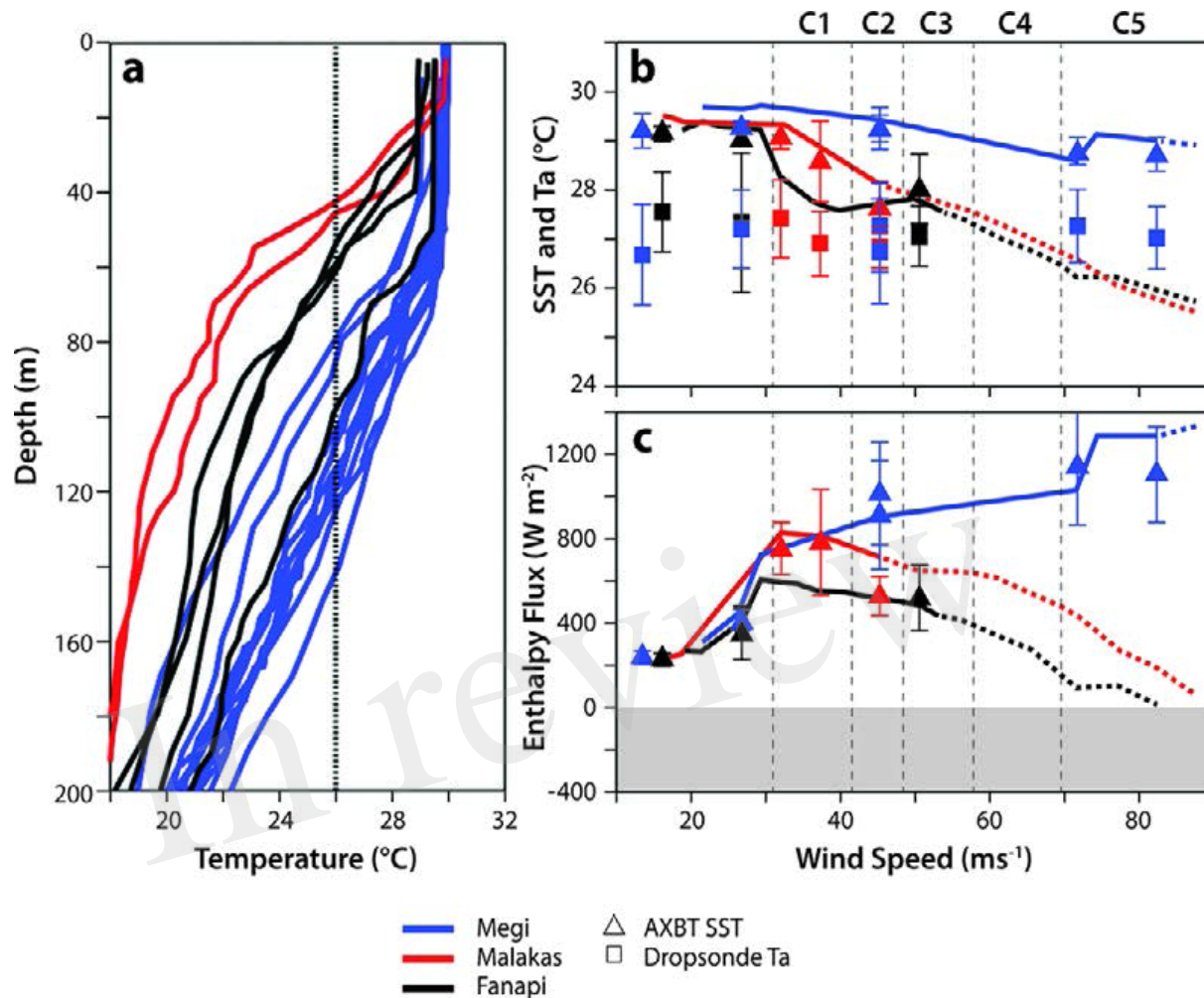
1371



1372
 1373
 1374
 1375
 1376
 1377
 1378
 1379

Figure 10. Background color map of average temperature for the upper 100 m (T100) from the East Asia Seas Nowcast/Forecast System on 23 September 2010. Overlaid are graphical representations of the ITOP operations area, experimental tools, and strategy. Locations of the three major ITOP storms at the time of maximum sampling are shown by storm symbols. Figure originally from D'Asaro et al. (2014), ©American Meteorological Society. Used with permission.

1380



1381

1382

1383 **Figure 11.** Evolution of temperature and air–sea fluxes for three ITOP TCs (Megi, Fanapi, and

1384 Malakas). (a) Pre-TC temperature profiles from ARGO floats. (b) Symbols: SST and air

1385 temperature at the core of each TC as measured by dropsonde/AXBT pairs. Lines: results of an

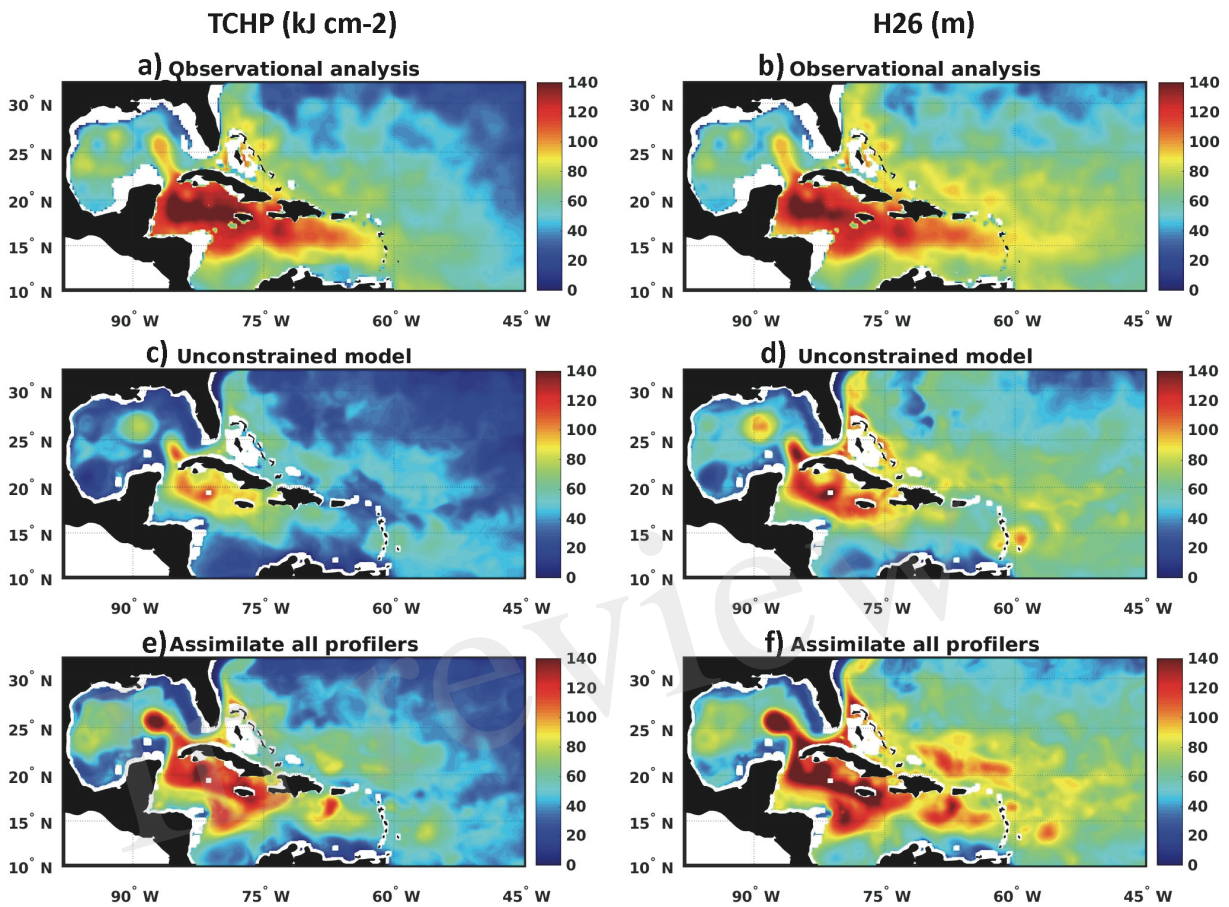
1386 ocean model (Price et al., 1994) driven by the observed TC (solid) and extrapolated to higher

1387 wind speeds (dashed). (c) As in (b), but for estimated total enthalpy flux. Reproduced from Lin

1388 et al., (2013).

1389

1390

1391
1392

1393 **Figure 12.** Mean fields of TCHP (a, c, and e) and H₂₆ (b, d, and f) averaged over the time
 1394 interval 21 August through 8 October 2017. Observation-based estimates are provided by the
 1395 NOAA/AOML TCHP product (a and b). Model fields are from an unconstrained simulation (c
 1396 and d) and from an analysis that assimilated all ocean profilers (Argo floats, underwater gliders,
 1397 and Alamo floats).

Figure 1.JPEG

In review

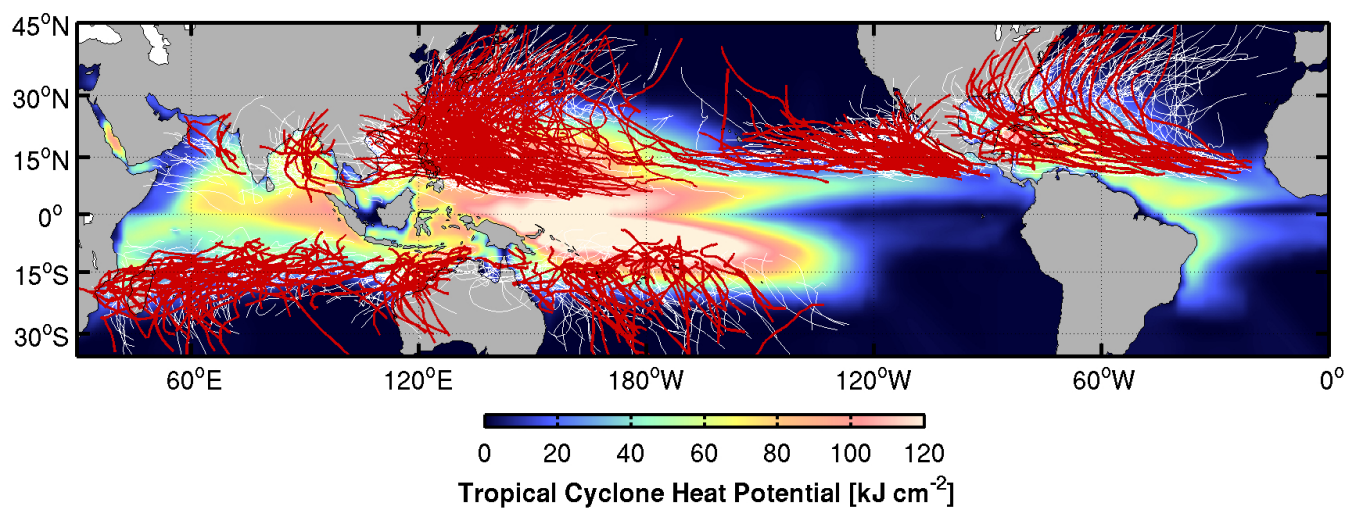


Figure 2.JPEG

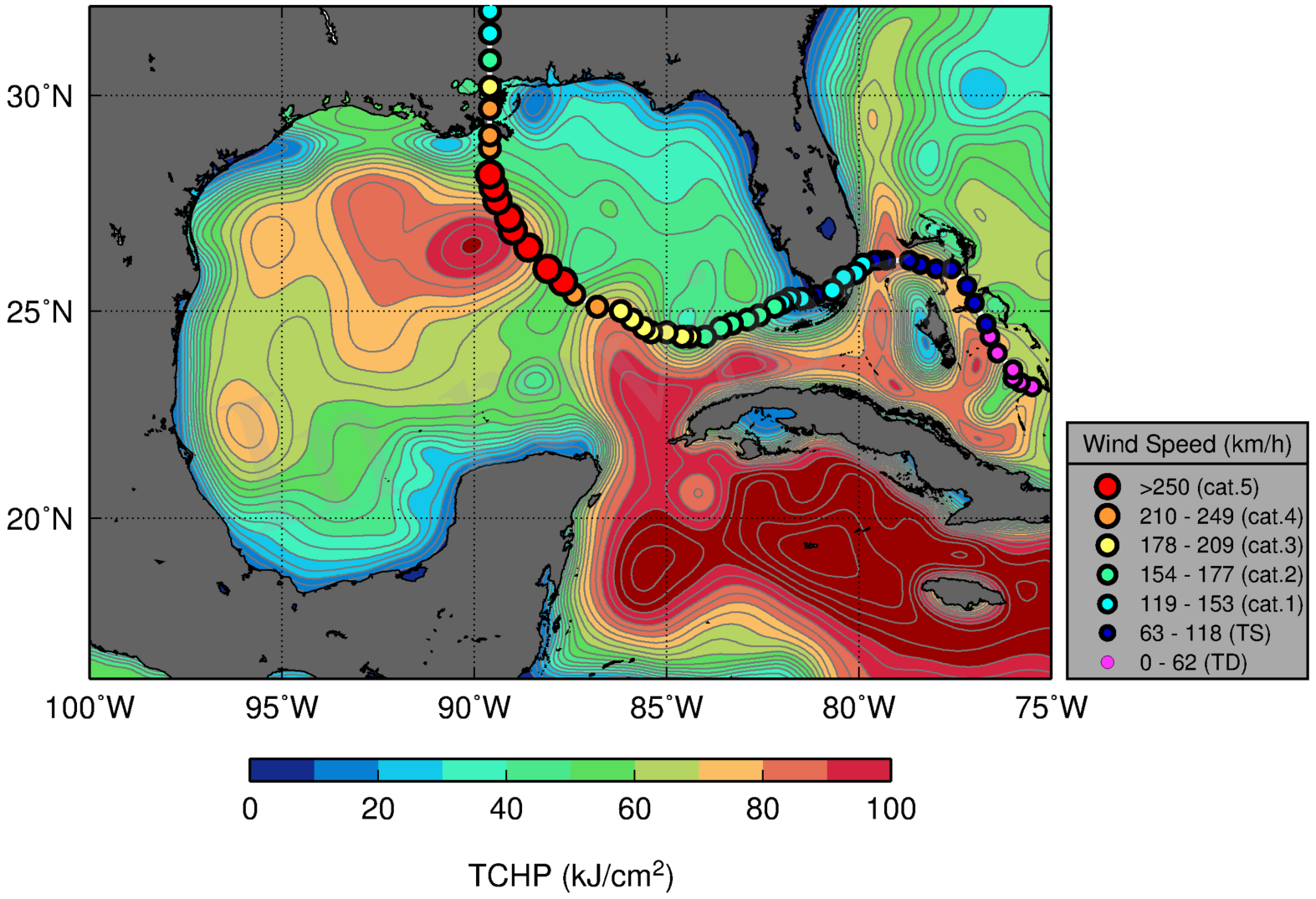


Figure 3.JPEG

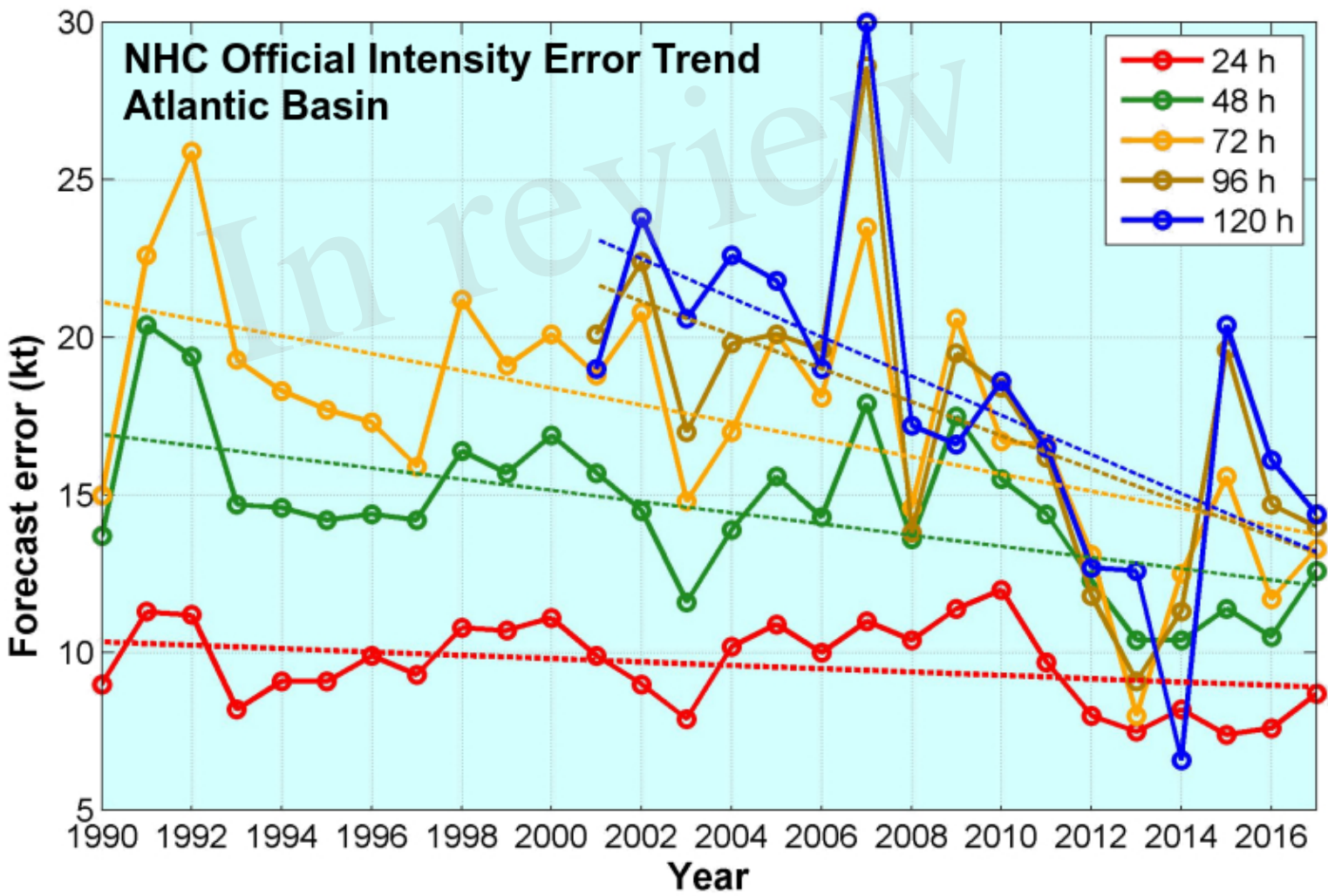
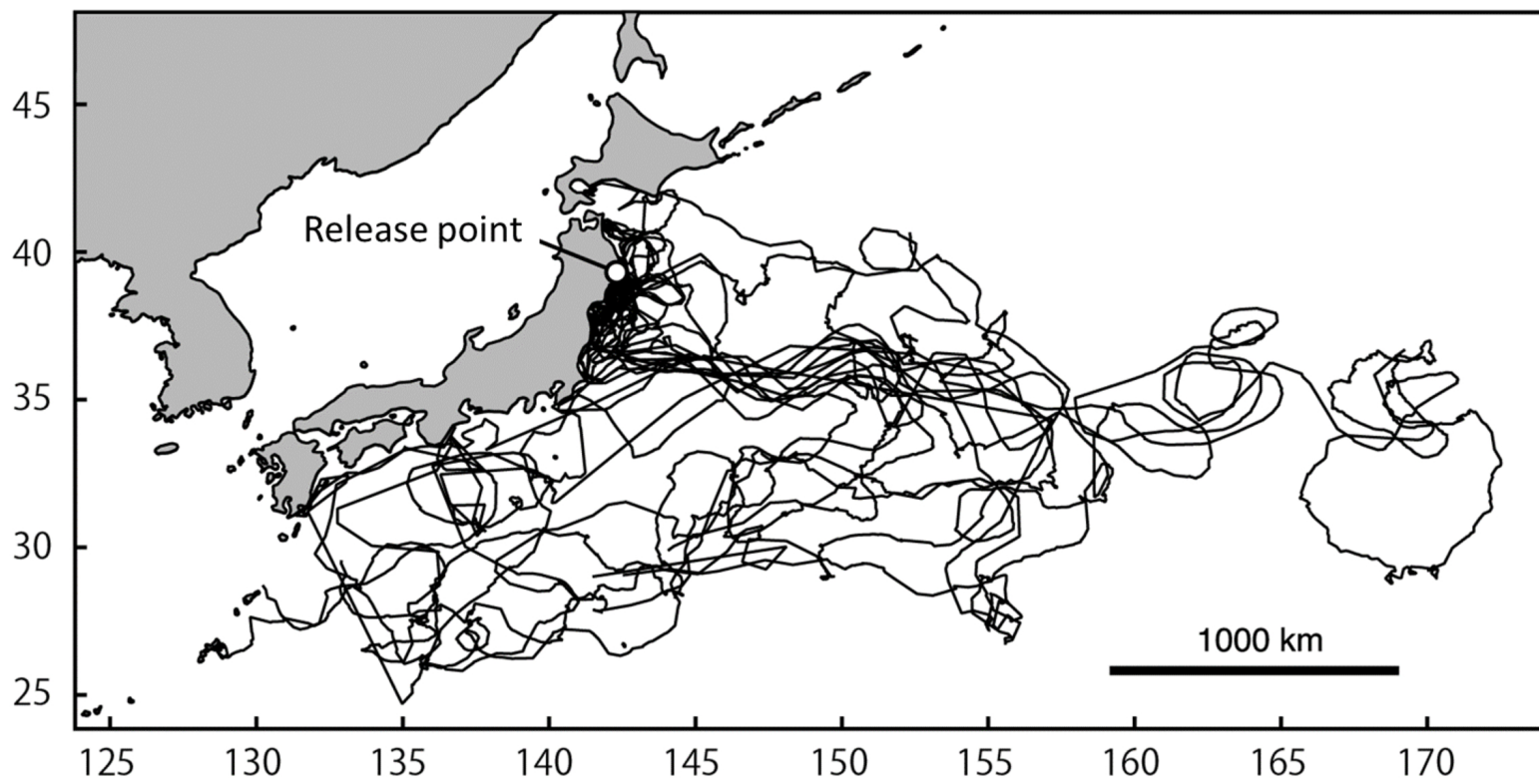


Figure 4.JPEG

(a)



(b)

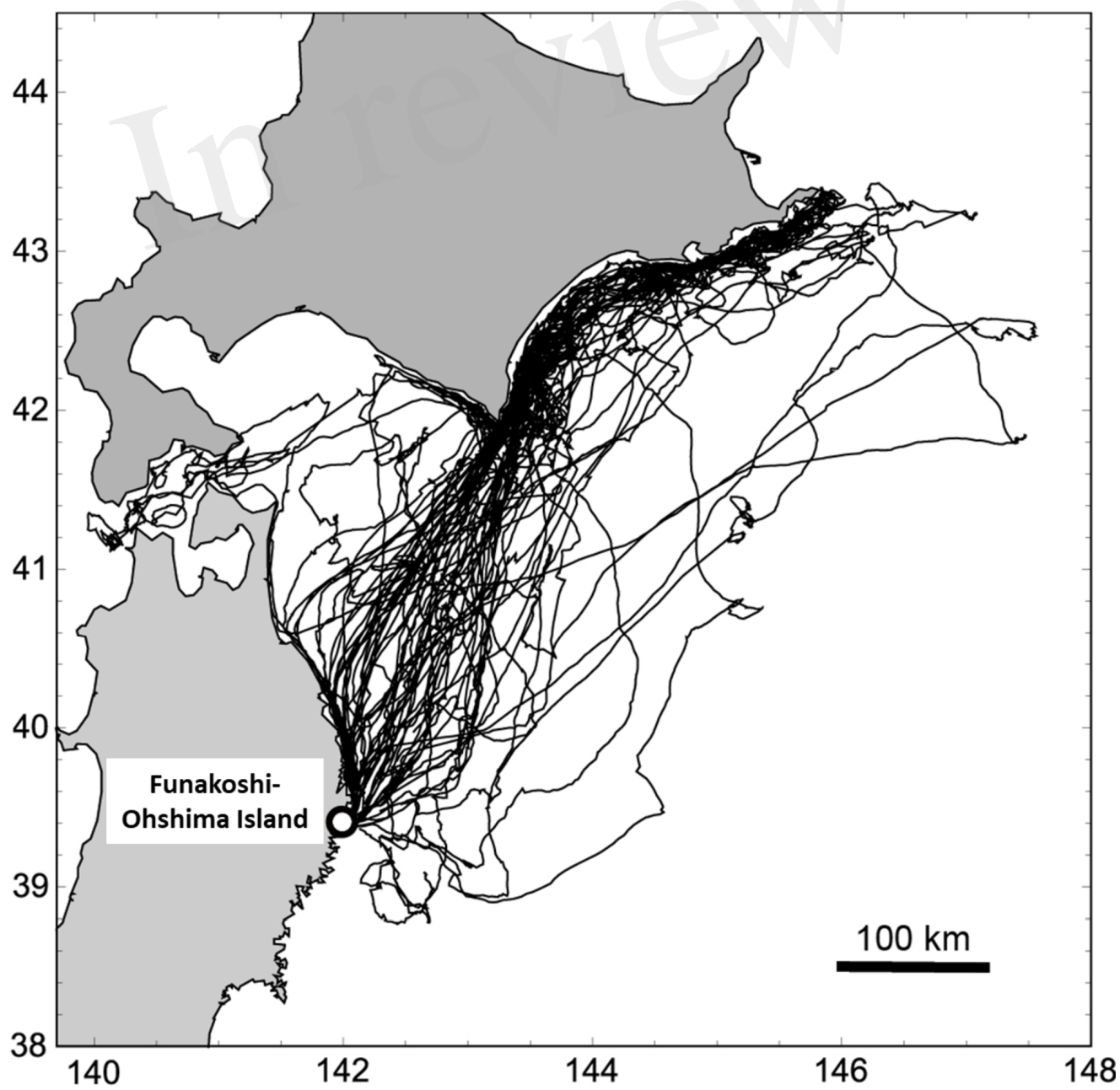


Figure 5.JPEG

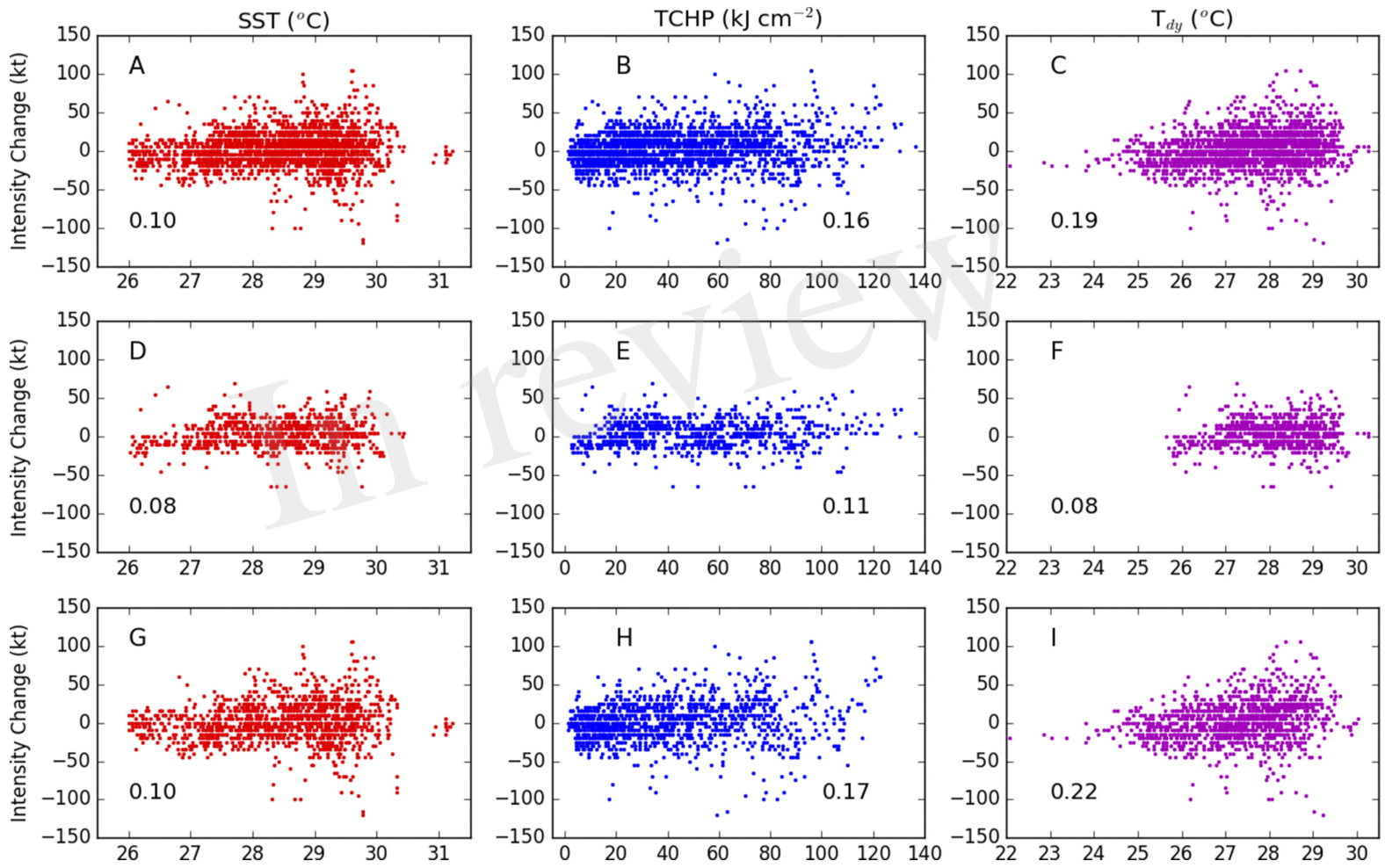


Figure 6.JPEG

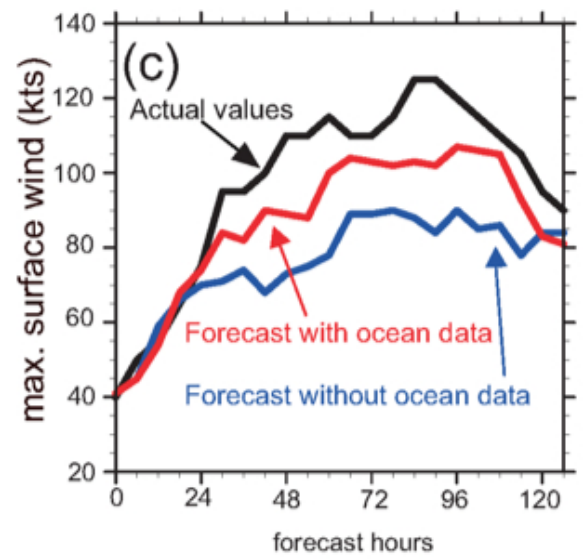
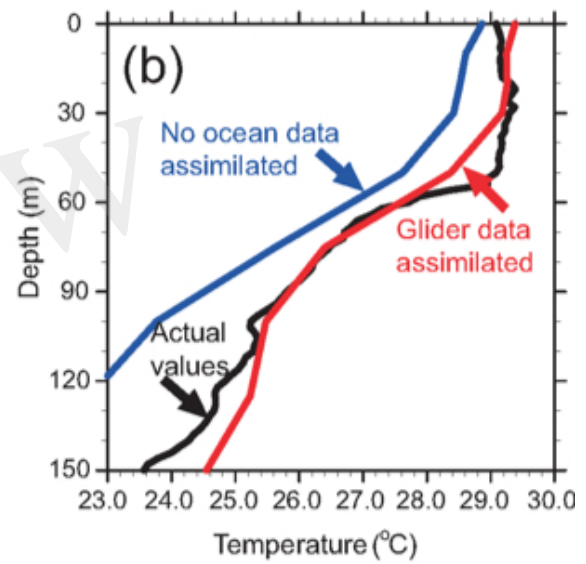
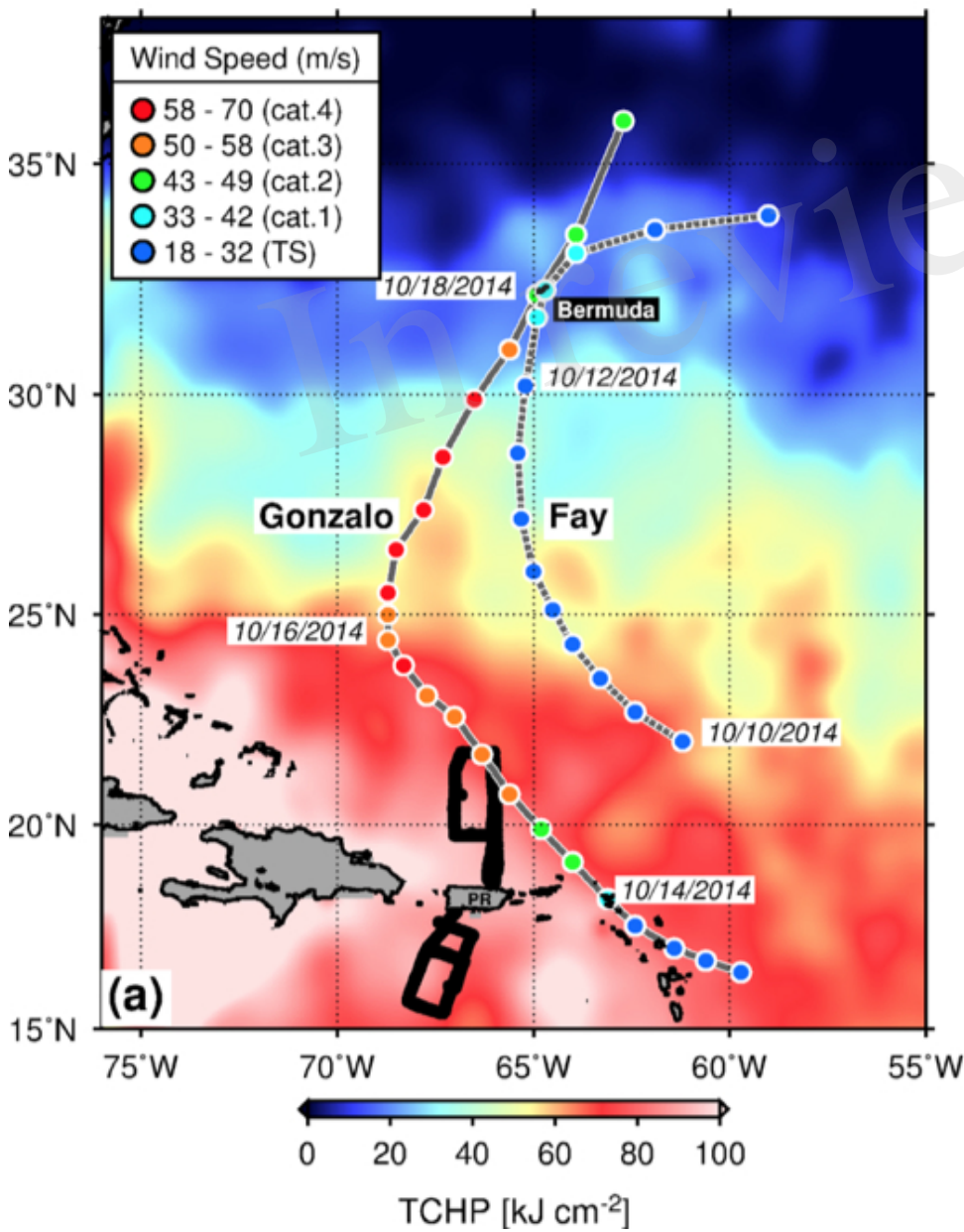


Figure 7.JPEG

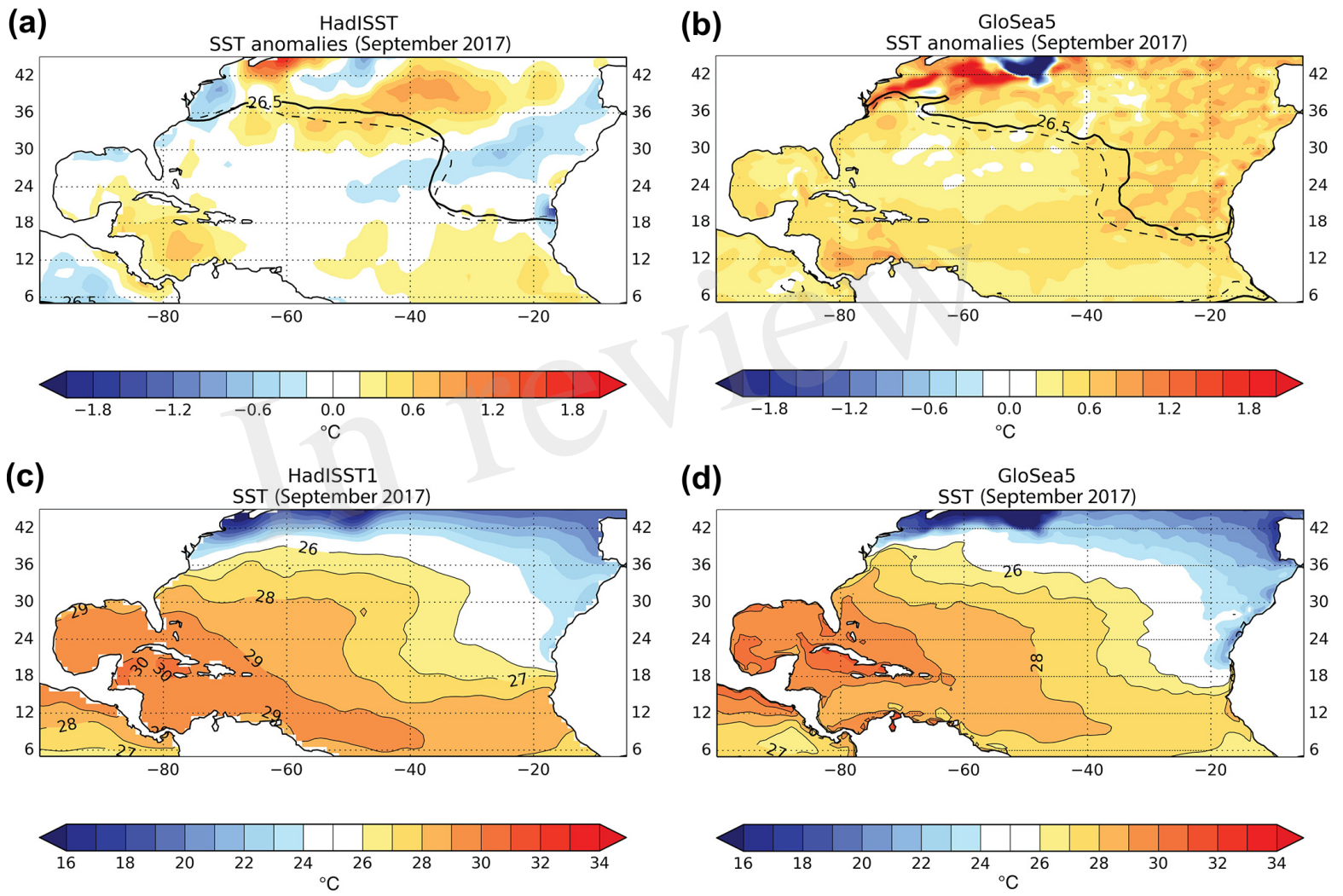


Figure 8.JPEG

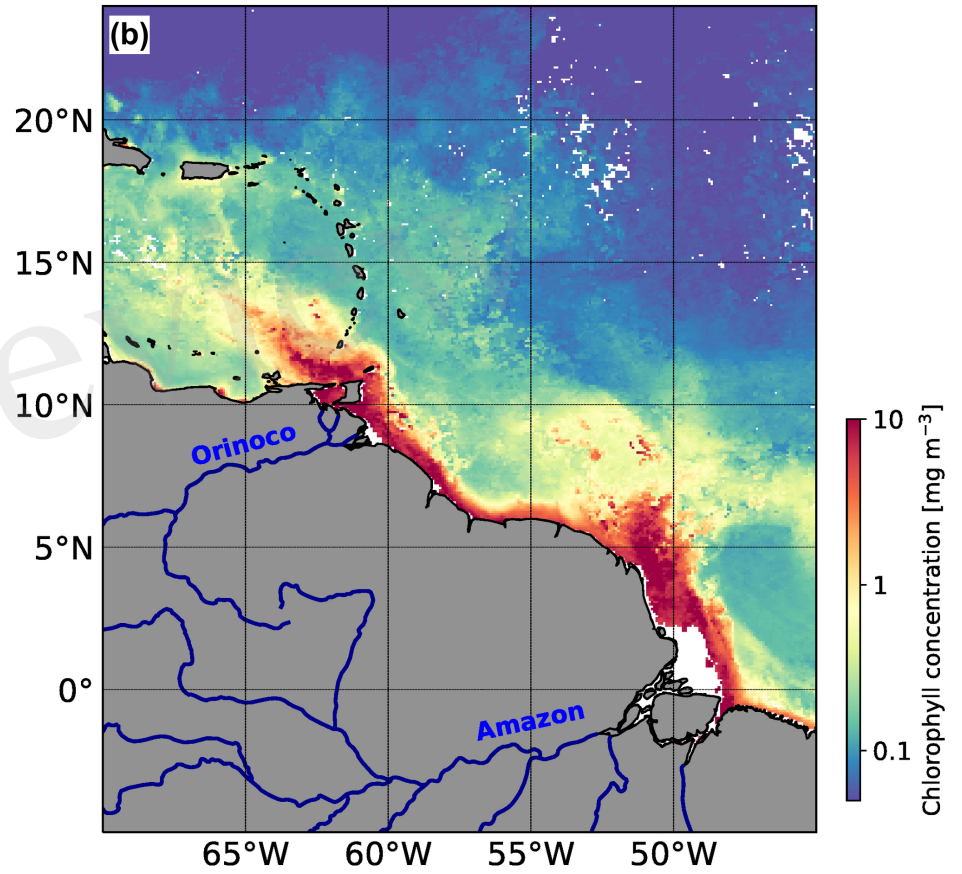
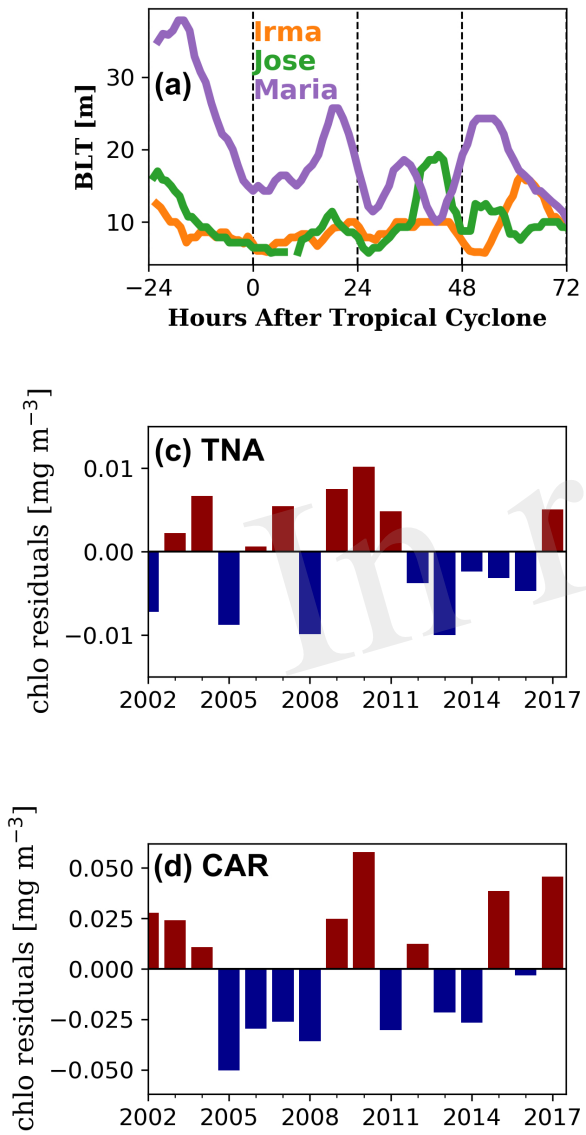


Figure 9.JPEG

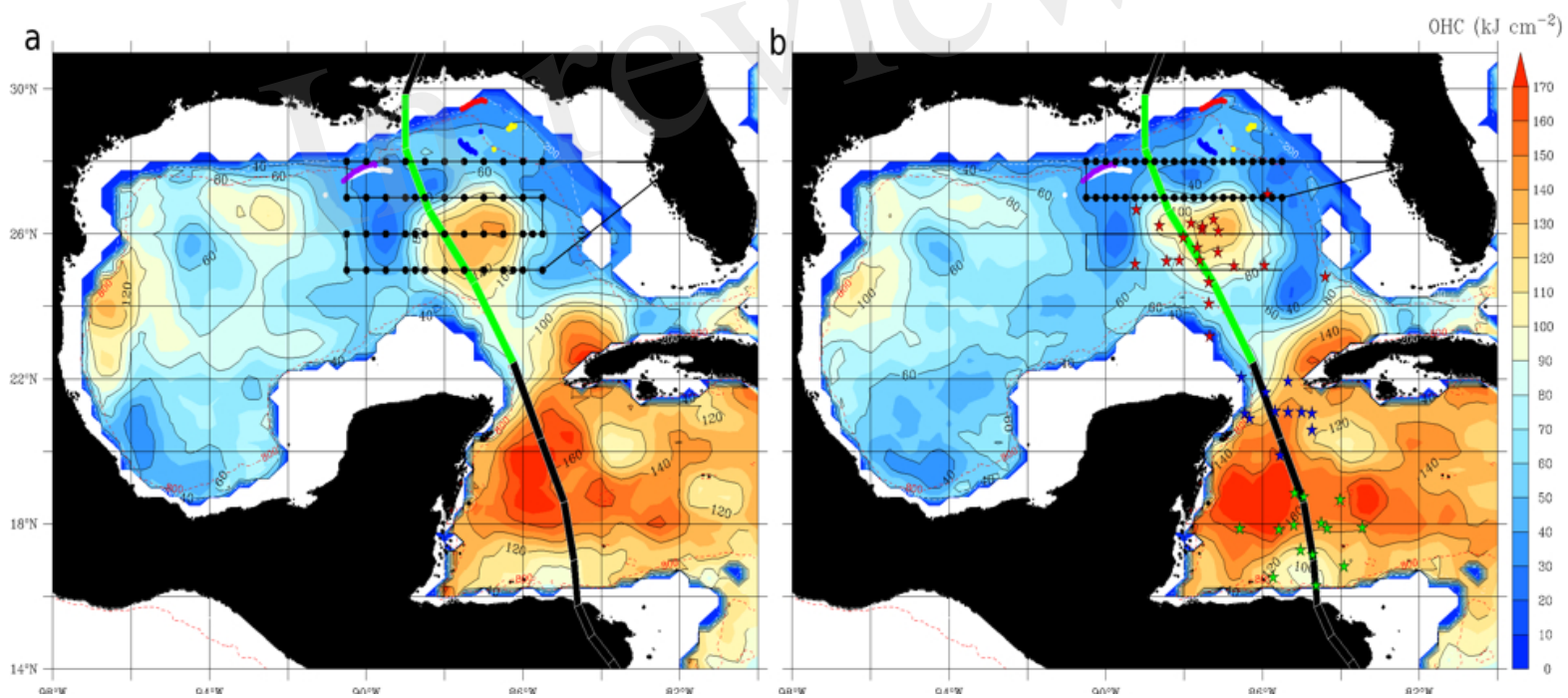


Figure 10.TIF

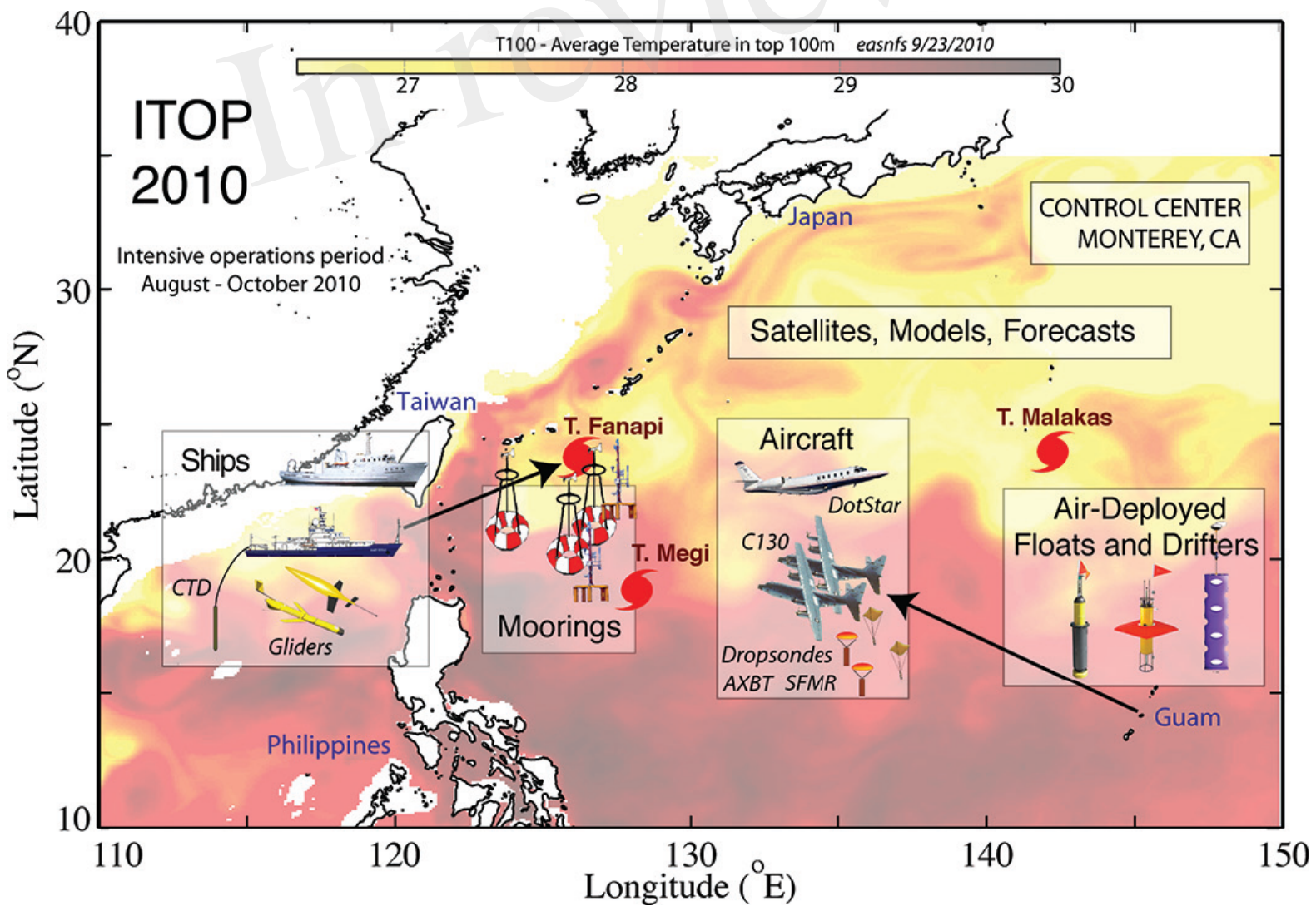
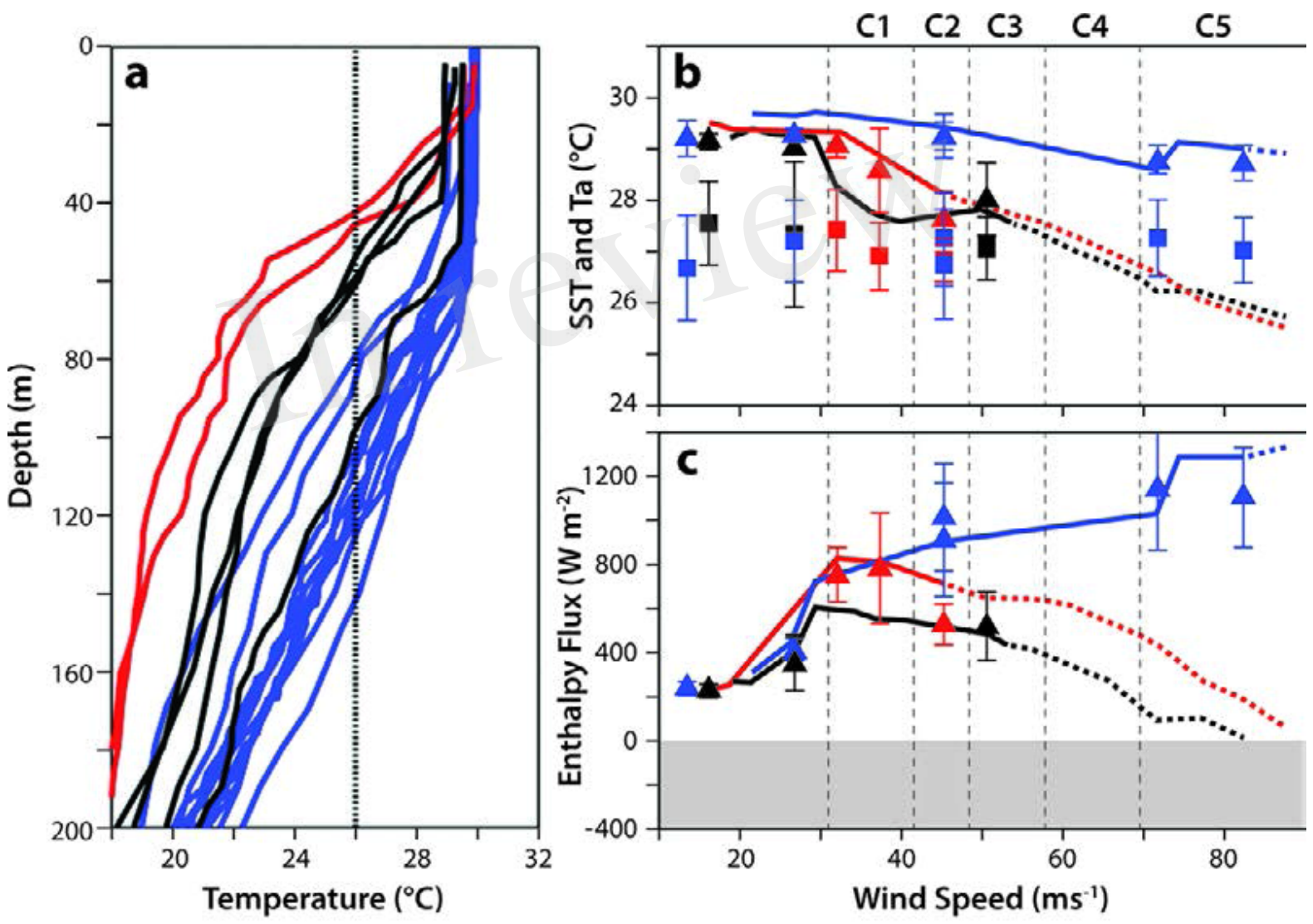


Figure 11.TIF



- Megi
- Malakas
- Fanapi
- AXBT SST
- Dropsonde Ta

Figure 12.JPEG

